



Jefferson Lab PAC25 Proposal Cover Sheet

This document must be received by close of business Tuesday, December 2, 2003 at:

Jefferson Lab
User/International Liaison
Mail Stop 12B
12000 Jefferson Ave.
Newport News, VA
23606

Experimental Hall: C

Days Requested for Approval: 37

Proposal Title:

The Neutron Electric Form Factor at Higher Q^2 up to 4.0 (GeV/c)^2 from the Reaction $^2\text{H}(e, e' n)^1\text{H}$ via Recoil Polarimetry

Proposal Physics Goals

Indicate any experiments that have physics goals similar to those in your proposal.

Approved, Conditionally Approved, and/or Deferred Experiment(s) or proposals:

E02-013 for Gen/Gmn

Contact Person

Name: Richard Madey

Institution: Kent State University & Jefferson Lab

Address: Kent, OH 44242 &

Address: Newport News, VA 23606

City, State, ZIP/Country: USA

Phone: (757) 269-7323

Fax: (757) 269-6273

E-Mail: madey@jlab.org

Jefferson Lab Use Only

Receipt Date: _____

By: _____

LAB RESOURCES LIST

JLab Proposal No.: _____
(For JLab ULO use only.)

Date December 01, 2003

List below significant resources — both equipment and human — that you are requesting from Jefferson Lab in support of mounting and executing the proposed experiment. Do not include items that will be routinely supplied to all running experiments such as the base equipment for the hall and technical support for routine operation, installation, and maintenance.

Major Installations (*either your equip. or new equip. requested from JLab*)

- Neutron Polarimeter & Enclosure
- Dipole Magnet [Charybdis]
- Steel Shadow Shield
- Lead Curtain

New Support Structures:

- Shield House & Collimator for Polarimeter
- Support Structure for Polarimeter
- Support Structure for Shadow Shield

Data Acquisition/Reduction

Computing Resources:

New Software:

Major Equipment

Magnets: -HMS
-Charybdis

Power Supplies: -HMS
-SOS [for Charybdis]

Targets: -LD2
-LH2
-Dummy

Detectors: -Additional Detectors for Polarimeter
-Replacement PMTs for Polarimeter Detectors

Electronics: -Quad Constant-Fraction Discriminators
-Delay Lines

Computer Hardware:

Other: -Moeller Polarimeter
-Compton Polarimeter, if available

Other:

BEAM REQUIREMENTS LIST

JLab Proposal No.: _____ Date: December 01, 2003

Hall: c Anticipated Run Date: _____ PAC Approved Days: _____

Spokesperson: Richard Madey

Hall Liaison: _____

Phone: (757) 269-7323

E-mail: madey@jlab.org

List all combinations of anticipated targets and beam conditions required to execute the experiment. (This list will form the primary basis for the Radiation Safety Assessment Document (RSAD) calculations that must be performed for each experiment.)

Condition No.	Beam Energy (MeV)	Mean Beam Current (μA)	Polarization and Other Special Requirements (e.g., time structure)	Target Material (use multiple rows for complex targets — e.g., w/windows)	Material Thickness (mg/cm^2)	Est. Beam-On Time for Cond. No. (hours)
1	3682	75	$\geq 80\%$ Polarization	15-cm LD2	2430	168
2	3682	90	$\geq 80\%$ Polarization	15-cm LH2	1065	24
3	3682	1	$\geq 80\%$ Polarization	Fe	8	24
4	3682	10	$\geq 80\%$ Polarization	15-cm LD2	2430	36
5	3682	75	$\geq 80\%$ Polarization	Al	583	24
6	5612	55	$\geq 80\%$ Polarization	15-cm LD2	2430	504
7	5612	90	$\geq 80\%$ Polarization	15-cm LH2	1065	24
8	5612	1	$\geq 80\%$ Polarization	Fe	8	24
9	5612	10	$\geq 80\%$ Polarization	15-cm LD2	2430	36
10	5612	55	$\geq 80\%$ Polarization	Al	583	24

The beam energies, E_{Beam} , available are: $E_{\text{Beam}} = N \times E_{\text{Linac}}$ where $N = 1, 2, 3, 4, \text{ or } 5$. $E_{\text{Linac}} = 800 \text{ MeV}$, i.e., available E_{Beam} are 800, 1600, 2400, 3200, and 4000 MeV. Other energies should be arranged with the Hall Leader before listing.

HAZARD IDENTIFICATION CHECKLIST

JLab Proposal No.: _____

Date : December 01, 2003

(For JLab U/I Liaison Office use only.)

Check all items for which there is an anticipated need.

<p>Cryogenics</p> <p><input type="checkbox"/> beamline magnets</p> <p><input type="checkbox"/> analysis magnets</p> <p><input checked="" type="checkbox"/> target type: <u>LD2, LH2</u> flow rate: _____ capacity: _____</p>	<p>Electrical Equipment</p> <p><input type="checkbox"/> cryo/electrical devices</p> <p><input type="checkbox"/> capacitor banks</p> <p><input checked="" type="checkbox"/> high voltage</p> <p><input type="checkbox"/> exposed equipment</p>	<p>Radioactive/Hazardous Materials</p> <p>List any radioactive or hazardous/toxic materials planned for use:</p>
<p>Pressure Vessels</p> <p>_____ inside diameter</p> <p>_____ operating pressure</p> <p>_____ window material</p> <p>_____ window thickness</p>	<p>Flammable Gas or Liquids</p> <p>type: _____</p> <p>flow rate: _____</p> <p>capacity: _____</p> <p>Drift Chambers</p> <p>type: _____</p> <p>flow rate: _____</p> <p>capacity: _____</p>	<p>Other Target Materials</p> <p><input type="checkbox"/> Beryllium (Be)</p> <p><input type="checkbox"/> Lithium (Li)</p> <p><input type="checkbox"/> Mercury (Hg)</p> <p><input type="checkbox"/> Lead (Pb)</p> <p><input type="checkbox"/> Tungsten (W)</p> <p><input type="checkbox"/> Uranium (U)</p> <p><input type="checkbox"/> * Helium (³He)</p> <p><input checked="" type="checkbox"/> Other (list below) -Aluminum Dummy -Fe (for Moeller Polarimeter)</p> <p>* U/I Liaison Office to notify RADCON</p>
<p>Vacuum Vessels</p> <p>_____ inside diameter</p> <p>_____ operating pressure</p> <p>_____ window material</p> <p>_____ window thickness</p>	<p>Radioactive Sources</p> <p><input type="checkbox"/> permanent installation</p> <p><input checked="" type="checkbox"/> temporary use</p> <p>type: <u>228 Thorium</u></p> <p>strength: <u>~10 uC</u></p>	<p>Large Mech. Structure/System</p> <p><input type="checkbox"/> lifting devices</p> <p><input type="checkbox"/> motion controllers</p> <p><input checked="" type="checkbox"/> scaffolding or</p> <p><input checked="" type="checkbox"/> elevated platforms</p>
<p>Lasers</p> <p>type: _____</p> <p>wattage: _____</p> <p>class: _____</p> <p>Installation:</p> <p><input type="checkbox"/> permanent</p> <p><input type="checkbox"/> temporary</p> <p>Use:</p> <p><input type="checkbox"/> calibration</p> <p><input type="checkbox"/> alignment</p>	<p>Hazardous Materials</p> <p><input type="checkbox"/> cyanide plating materials</p> <p><input type="checkbox"/> scintillation oil (from)</p> <p><input type="checkbox"/> PCBs</p> <p><input type="checkbox"/> methane</p> <p><input type="checkbox"/> TMAE</p> <p><input type="checkbox"/> TEA</p> <p><input type="checkbox"/> photographic developers</p> <p><input type="checkbox"/> other (list below)</p>	<p>General</p> <p>Experiment Class:</p> <p><input type="checkbox"/> Base Equipment</p> <p><input type="checkbox"/> Temp. Mod. to Base Equip.</p> <p><input type="checkbox"/> Permanent Mod. to Base Equipment</p> <p><input checked="" type="checkbox"/> Major New Apparatus</p> <p>Other: Polarimeter</p>

Computing Requirements List

Proposal Title: The Neutron Electric Form Factor at Higher Q^2 up to 4.0 (GeV/c)² from the Reaction $^2\text{H}(e, e' n)^1\text{H}$ via Recoil Polarimetry

Spokesperson: Richard Madey **Experimental Hall:** C

Raw Data Expected

Total: 1500 GB **Per Year (long duration experiments only):** _____

Simulation Compute Power (SPECint95 hours) Required: 2000 hours CPU on Linux farm

On-Line Disk Storage Required: 600 GB work space

Imported Data Amount from Outside Institutions: _____

Exported Data Amount to Outside Institutions: _____

Expected Mechanism for Imported/Exported Data: _____

Special Requirements

For example, special configuration of data acquisition systems) that may require resources and/or coordination with JLab's Computer Center. Please indicate, if possible, what fraction of these resources will be provided by collaborating institutions and how much is expected to be provided by JLab.

Submit

**The Neutron Electric Form Factor at Higher
 Q^2 up to 4.0 (GeV/c)² from the Reaction
 ${}^2H(\vec{e}, e'\vec{n}){}^1H$ via Recoil Polarimetry**

Spokesman: R. Madey, Kent State University

Co-Spokesman: S. Kowalski, MIT

Co-Spokesman: A. Yu. Semenov, Kent State University

Co-Spokesman: B. D. Anderson, Kent State University

Abstract

We propose to extend measurements of the electric form factor of the neutron, G_E^n , to a squared four-momentum transfer of 4.0 (GeV/c)². The JLab E93-038 collaboration conducted $d(\vec{e}, e'\vec{n})p$ measurements on a liquid deuterium target at Q^2 values of 0.45, 1.13, and 1.45 (GeV/c)². *Polarization measurements above $Q^2 \approx 1$ (GeV/c)² require the beam energies available at CEBAF. In the technique demonstrated in E93-038 with a high-luminosity, high-efficiency neutron polarimeter and the dipole neutron-spin-precession magnet [Charybdis], we measured the ratio of two scattering asymmetries associated with positive and negative precessions of the neutron polarization vector.* In this ratio technique, systematic uncertainties are small because the analyzing power of the polarimeter cancels in the ratio, and the beam polarization cancels also because, as demonstrated in E93-038, the beam polarization does not change much in sequential measurements of the two scattering asymmetries.

The primary motivation for this measurement is the ability to measure a fundamental quantity of the neutron – one of the basic building blocks of matter. Because our method is sensitive to the sign of G_E^n , the proposed experiment will determine the sign of G_E^n in the region 2 to 4 (GeV/c)², which is crucial for disentangling the structure of the nucleon. A successful model of confinement must be able to predict both neutron and proton electromagnetic form factors simultaneously. The neutron electric form factor is especially sensitive to small components of the nucleon wave function, and differences between model predictions for G_E^n tend to increase rapidly with Q^2 . The proposed measurements of G_E^n will be available to distinguish models and to challenge rigorous Lattice QCD calculations. These measurements of G_E^n are needed to understand electron scattering experiments that probe electric structure functions at high Q^2 ; it is important for the analysis of few-body data from measurements at Jefferson Lab. Nuclear physics corrections [for FSI, MEC, and IC] are more reliable for the deuteron than for helium; also, the reaction mechanism is expected to be simpler in deuterium than in helium.

List of Participants

R. Madey (Spokesman), B.D. Anderson (Co-Spokesman and Institutional Representative),
A.R. Baldwin, D.M. Manley, A.Yu. Semenov (Co-Spokesman), I.A. Semenova, J.W. Watson,
W.-M. Zhang, Graduate Student

Kent State University

R. Carlini (Institutional Representative), R. Ent, H. Fenker, M. Jones, D. Higinbotham,
D. Mack, G. Smith, W. Vulcan, B. Wojtsekhowski, S. Wood, C. Yan

Thomas Jefferson National Accelerator Facility

S. Kowalski (Co-Spokesman and Institutional Representative), M. Farkhondeh, S. Taylor

Massachusetts Institute of Technology

C. Howell (Institutional Representative), S. Tajima, Postdoc

Duke University

H. Breuer, J.J. Kelly (Institutional Representative), N. Savvinov

University of Maryland

E. Crouse, J.M. Finn (Institutional Representative), C. Perdrisat

The College of William and Mary

O.K. Baker (Institutional Representative), E. Christy, L. Cole, P. Gueye, B. Hu, C. Keppel,
L. Tang, L. Yuan

Hampton University

A. Ahmidouch (Institutional Representative), S. Danagoulian, A. Gasparian

North Carolina A&T State University

G. MacLachlan, A. Opper (Institutional Representative)

Ohio University

List of Participants (continued)

A. Aghalaryan, R. Asaturyan, H.G. Mkrtchyan (Institutional Representative), S. Stepanyan,
V. Tadevosyan

Yerevan Physics Institute

S. Wells (Institutional Representative), N. Simicevic

Louisiana Tech

P. Markowitz (Institutional Representative), B. Raue, J. Reinhold

Florida International University

D. Day (Institutional Representative), F. Wesselmann, H. Zhu

University of Virginia

W. Tireman

James Madison University

P. Ulmer

Old Dominion University

M. Khandaker (Institutional Representative), V. Punjabi

Norfolk State University

M. Elaasar

Southern University at New Orleans

R.E. Segel

Northwestern University

R. Wilson

Harvard University

List of Participants (continued)

W.-Y. Kim (Institutional Representative), Graduate Student

Kyungpook National University

T. Reichelt

University of Bonn

L. Gan

University of North Carolina at Wilmington

H. Arenhovel

University of Mainz

B. Plaster

California Institute of Technology

Contents

	<u>Page</u>
Abstract	i
List of Participants	ii
Contents	v
List of Figures	vi
List of Tables	vii
1 Scientific Motivation and Background	1
1.1 Extension of E93-038 to Measure G_E^n at Q^2 up to 4.0 (GeV/c)^2	1
1.2 Better Understanding of Nucleon Structure	3
1.3 Better Understanding of Electron Scattering Data from Nuclei	6
1.4 Nuclear Physics Corrections and Reaction Mechanism Questions	8
2 Theoretical Background	9
3 Description of the Experiment	10
3.1 Experimental Arrangement	10
3.2 Kinematics	13
3.3 Count Rates	13
3.4 Projected Uncertainties	14
4 Some Results from E93-038	20
5 Beam Time	26
6 Collaboration	27
References	29
Appendix A: <i>R. Madey et al., Measurements of G_E^n/G_M^n from the ${}^2\text{H}(\vec{e}, e' \vec{n}){}^1\text{H}$ Reaction to $Q^2 = 1.45 \text{ (GeV/c)}^2$, <i>Phys. Rev. Lett.</i> <u>91</u>, 122002 (2003)</i>	33

List of Figures

1	G_E^n versus Q^2 . The dashed line reflects the Galster parameterization; the solid line is our modified Galster fit.	1
2	G_E^n versus Q^2 . The dashed line reflects the Galster parameterization; the solid line is our modified Galster fit.	2
3	Predictions of selected models (see text for descriptions and the legend) for $\mu_p G_E^p/G_M^p$ and $\mu_n G_E^n/G_M^n$ compared with proton and neutron data. The neutron data symbols are the same as in Fig. 1.	4
4	Predictions of the 1973 model (dashed) by Iachello, Jackson, and Lande, and the 2003 model (solid) by Bijker and Iachello for $\mu_p G_E^p/G_M^p$ (top panel) and $\mu_n G_E^n/G_M^n$ (bottom panel) compared with proton and neutron data.	5
5	Proton and neutron form factors as a function of Q^2 . The red solid line in the top panel is a parameterization from Eq. (4) for G_E^p	7
6	The ratio of isoscalar and isovector cross-sections [Eq. (6)] as a function of Q^2 . We assume the modified Galster parameterization for G_E^n and the parameterization from Eq. (4) for G_E^p	8
7	Comparison of the final results for G_E^n extracted from analyses assuming $n(\vec{e}, e'\vec{n})$ elastic scattering and a point acceptance (black triangles), the acceptance-averaged ${}^2\text{H}(\vec{e}, e'\vec{n}){}^1\text{H}$ Arenhövel PWBA model (red circles), and the acceptance-averaged ${}^2\text{H}(\vec{e}, e'\vec{n}){}^1\text{H}$ Arenhövel FSI+MEC+IC model (blue squares). The error bars shown are the quadrature sum of the statistical and systematic errors, and the solid curve is the Galster parameterization.	9
8	Schematic diagram of the experimental arrangement in E93-038.	11
9	Neutron polarimeter to be used in the measurements.	12
10	Singles rates for beam energy of 884 MeV and a CHARYBDIS current of -170 A.	13
11	Simulated spectra of the particles at 31.6° behind 4-in Pb curtain from 3.682 GeV electron beam incident on a 15-cm LD_2 target.	16
12	Simulated spectra of the particles at 31.6° behind 4-in Pb curtain from 5.612 GeV electron beam incident on a 15-cm LD_2 target.	17
13	Calculated fraction of electron-neutron coincidence events corrupted from a background particle (charged or neutral) that appears during the coincidence time window of 20 ns as a function of the beam current.	18
14	Top (bottom) panels: Projected uncertainties $\Delta g_n/g_n$ and ΔG_E^n at $Q^2 = 3.0$ (4.0) $(\text{GeV}/c)^2$ as a function of the DAQ time for a beam current of 75 (55) μA	19
15	Statistical uncertainty $\Delta g/g$, projected at $Q^2 = 3.0$ and 4.0 $(\text{GeV}/c)^2$, as a function of precession angle χ	20
16	Invariant mass spectra before and after cuts on the scattered electron momentum, the missing momentum, and an HMS-NPOL coincidence time-of-flight.	21
17	Typical time-of-flight spectra for $Q^2 = 1.45$ $(\text{GeV}/c)^2$. Selected portions are shaded.	22
18	Asymmetries obtained from the analysis of E93-038 data at $Q^2 = 1.13$ $(\text{GeV}/c)^2$	23
19	Histogram of E93-038 asymmetries at $Q^2 = 1.13$ $(\text{GeV}/c)^2$ ($\chi = 0^\circ$). The red solid curve is a Gaussian fit, and the blue dashed line is the mean value of the asymmetry from the Fig. 18.	24

20	Real event rate, accidental coincidence rate, and the reals-to-accidentals ratio obtained from E93-038. The target-front array flight path was 7 m for NPOL at 46 degrees.	25
21	Comparison of the simulated neutron polarimeter parameters (viz., analyzing power, A_Y , and the neutron polarimeter efficiency, ϵ_n) with the results from E93-038. Yellow band in the left panel shows an uncertainty on the fit of the simulated efficiencies with a polynomial function.	26
22	Electron beam polarization in March 2001.	27

List of Tables

1	Kinematic conditions at a neutron scattering angle of 31.6° . Also listed is the Charybdis field integral $B\Delta l$ required to precess the neutron polarization vector.	14
2	The neutron polarimeter and HMS acceptances, estimated neutron polarimeter parameters, and calculated real event rate at $Q^2 = 3.0$ and 4.0 $(\text{GeV}/c)^2$ for a beam current of 75 and 55 μA , respectively, incident on a 15-cm LD_2 target. Also listed are the simulated NPOL efficiency and analyzing power (see Section 4 and Fig. 21 for details), and expected asymmetries for $-\chi$ and $+\chi$ precession of the neutron polarization vector.	15
3	Beam-time [days] for measuring at $Q^2 = 3.0$ and 4.0 $(\text{GeV}/c)^2$ for a 75 (55) μA , 80% polarized beam on a 15-cm LD_2 target.	28

1 Scientific Motivation and Background

1.1 Extension of E93-038 to Measure G_E^n at Q^2 up to 4.0 (GeV/c)²

The electric form factor of the neutron, G_E^n , is a fundamental quantity needed for the understanding of both nucleon and nuclear structure. The dependence of G_E^n on Q^2 reflects the distribution of charge in the neutron. The E93-038 collaboration carried out measurements of G_E^n from September 8, 2000 to April 26, 2001 at three values of Q^2 [viz., 0.45, 1.13, and 1.45 (GeV/c)²]. Results were reported in Physical Review Letters [Madey et al. (2003)], which is Appendix A of this proposal. Data from E93-038 are plotted (as filled squares) in Fig. 1 together with the current world data extracted from polarization measurements [Eden et al. (1994), Herberg et al. (1999), Bermuth et al. (2003), Golak et al. (2001), Passchier et al. (1999), Zhu et al. (2001)] and from an analysis of the deuteron quadrupole form factor [Schiavilla and Sick (2001)]. We fitted these data and the G_E^n slope at the origin as measured via low-energy neutron scattering from electrons in heavy atoms [Kopecky et al. (1997)] to a Galster et al. (1971) parameterization:

$$G_E^n = -a\mu_n\tau G_D/(1 + b\tau), \quad (1)$$

where $\tau = Q^2/4M_n^2$, $G_D = (1 + Q^2/\Lambda^2)^{-2}$, and $\Lambda^2 = 0.71$ (GeV/c)². Our best-fit parameters are $a = 0.886 \pm 0.023$ and $b = 3.29 \pm 0.31$ [Kelly (2003)].

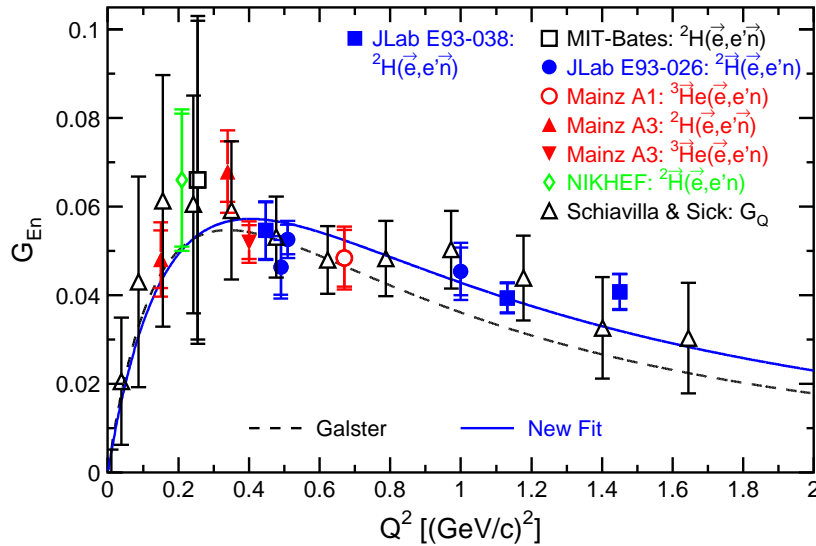


Figure 1: G_E^n versus Q^2 . The dashed line reflects the Galster parameterization; the solid line is our modified Galster fit.

We propose to extend measurements of G_E^n to 4.0 (GeV/c)². Shown on the Q^2 axis in Fig. 2 are projected uncertainties for proposed measurements from deuterium at $Q^2 = 3.0$ and 4.0 (GeV/c)². Also shown in Fig. 2 are three points [viz., $Q^2 = 1.3, 2.4,$ and 3.4 (GeV/c)²] to be measured in JLab E02-013 from a polarized ^3He target; the error bars here are from the proposal. Displayed in Fig. 2 are measurements made only at JLab.

Polarization measurements of G_E^n at Q^2 above ≈ 1 (GeV/c)² require the beam energies available at CEBAF. In the technique demonstrated in E93-038 with a high-luminosity, high-efficiency polarimeter and a dipole magnet ahead of the polarimeter to precess the spin of the

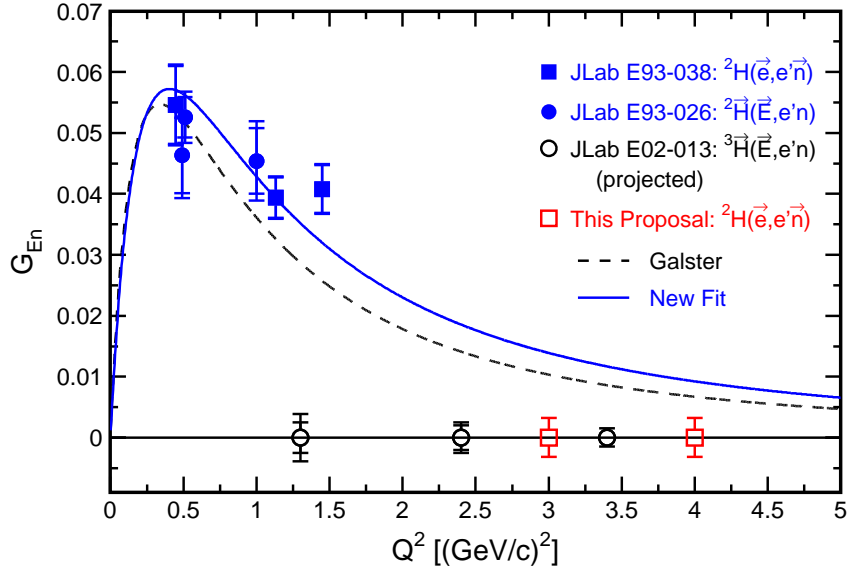


Figure 2: G_E^n versus Q^2 . The dashed line reflects the Galster parameterization; the solid line is our modified Galster fit.

neutron, we measured the ratio of two neutron scattering asymmetries: one asymmetry from precessing the neutron polarization vector in a positive direction; the other, from precessing it in a negative direction. In this ratio technique, systematic uncertainties are small because the analyzing power cancels in the ratio, and the beam polarization cancels also because, as demonstrated in E93-038, the beam polarization does not change much during the sequential measurements of the scattering asymmetries.

In the high Q^2 region above 1.5 (GeV/c)^2 , our present knowledge of the electric and magnetic form factors G_E and G_M for neutrons was obtained from measurements of the angular dependence of the cross section by quasielastic electron-deuteron scattering. Subtraction of the contribution from the proton in the deuteron introduces a large uncertainty. These previous experiments contain large systematic errors because of uncertainties in the theoretical description of the deuteron, mostly from final-state interactions (FSI) and meson-exchange currents (MEC). In the Q^2 region from 1.75 to 4.00 (GeV/c)^2 , Lung et al. (1993) reported measurements from SLAC-NE11 of quasielastic $e - d$ cross sections at forward and backward angles which permit a Rosenbluth separation of G_E^n and G_M^n at $Q^2 = 1.75, 2.50, 3.25,$ and 4.00 (GeV/c)^2 . Although Lung et al. (1993) stated that their data from SLAC-NE11 were consistent with $(G_E^n)^2 = 0$ for $1.75 < Q^2 \text{ (GeV/c)}^2 < 4.00$, these data appear consistent also with the modified Galster parameterization. The NE11 error bars do not permit distinguishing between $G_E^n = 0$ and the Galster parameterization.

In contrast to the Rosenbluth separation method, the polarization transfer method proposed here permits an experimental determination of the sign of G_E^n . This ability is another nice feature of the polarization transfer technique - especially in view of the fact that nothing is known about the sign of G_E^n at high Q^2 . Here we propose to measure G_E^n at higher Q^2 values of 3.0 and 4.0 (GeV/c)^2 with sufficient accuracy to challenge rigorous Lattice QCD calculations.

Negele (2000) is leading a major effort to use lattice QCD to understand the structure and interaction of hadrons. Fundamental lattice calculations will become available to solve QCD, the field theory of quarks and gluons. Currently, lattice calculations are limited by computer power; however, more computing power is expected to be available soon. Lattice QCD calculations are fundamental, whereas various model calculations are not. Lattice QCD has made impressive strides recently, with rigorous methods for separating hard and soft contributions and recent methods for extrapolation to the chiral limit for light quarks using explicit representations of nonanalytic contributions.

1.2 Better Understanding of Nucleon Structure

Measurements of G_E^n at high Q^2 will help us to understand the symmetry structure of nucleon electromagnetic form factors. Two symmetries play a crucial role: (1) relativistic invariance, which fixes the form of the nucleon current and hence the form of the form factors; and (2) isospin invariance, which gives relations between neutron and proton form factors. While relativistic invariance is expected to be exact, isospin invariance is not exact; however, it is expected to be only slightly broken in a realistic theory of the strong interaction. Isospin invariance leads to the introduction of isoscalar, F_{1S} and F_{2S} , and isovector, F_{1V} and F_{2V} , form factors, and hence to relations among proton and neutron form factors. The observed Sachs form factors, G_E^p and G_E^n , can be obtained from the relations:

$$G_E^p = (F_{1S} + F_{1V}) - \tau (F_{2S} + F_{2V}) \quad (2)$$

$$G_E^n = (F_{1S} - F_{1V}) - \tau (F_{2S} - F_{2V}) \quad (3)$$

where F_1 and F_2 are the Dirac and Pauli form factors. As a consequence of the two-term structure of Eqs. (2,3), with the second term being multiplied by $-Q^2/4M^2$, G_E^p and G_E^n may have zeros at some value of Q^2 , depending on the relative sign of the two terms.

Different models of the nucleon correspond to different assumptions for the Dirac and Pauli form factors. Models with a two-term structure produce results in qualitative agreement with data; for example, a soliton model [Holzwarth (2002)], two relativistic constituent quark models [Miller (2002) and Cardarelli and Simula (2002)], and a model [Lomon (2002)] that couples vector meson dominance with the predictions of pQCD all have this structure and produce results in qualitative agreement with data. Predictions of these models are compared with data in Fig. 3. The chiral soliton model [Holzwarth (2002)] reproduces the dramatic linear decrease observed in $\mu_p G_E^p/G_M^p$ for $1 < Q^2 < 6$ (GeV/c)²; however, this model fails to reproduce the neutron data at large Q^2 . A light-front calculation using pointlike constituent quarks surrounded by a cloud of pions [Miller(2002)], denoted ‘‘LFCBM’’, describes the neutron data, but falls below the proton data at high Q^2 . A one-gluon exchange light-front calculation, denoted ‘‘OGE CQM’’, using constituent quark form factors fitted to $Q^2 < 1$ (GeV/c)² data [Cardarelli and Simula (2000)] agrees with the neutron data, but deviates from the proton data above $Q^2 \sim 3.0$ (GeV/c)². The Lomon model, denoted ‘‘VMD + pQCD’’, agrees with the proton data but falls below the neutron data above $Q^2 \sim 1.2$ (GeV/c)².

In 1973, Iachello, Jackson, and Lande [1973] suggested that the structure of the nucleon consists of two components: (1) an intrinsic structure (presumably three valence quarks), and (2) a meson cloud parameterized in terms of vector mesons (ρ , ω , ϕ). In this 1973 model of

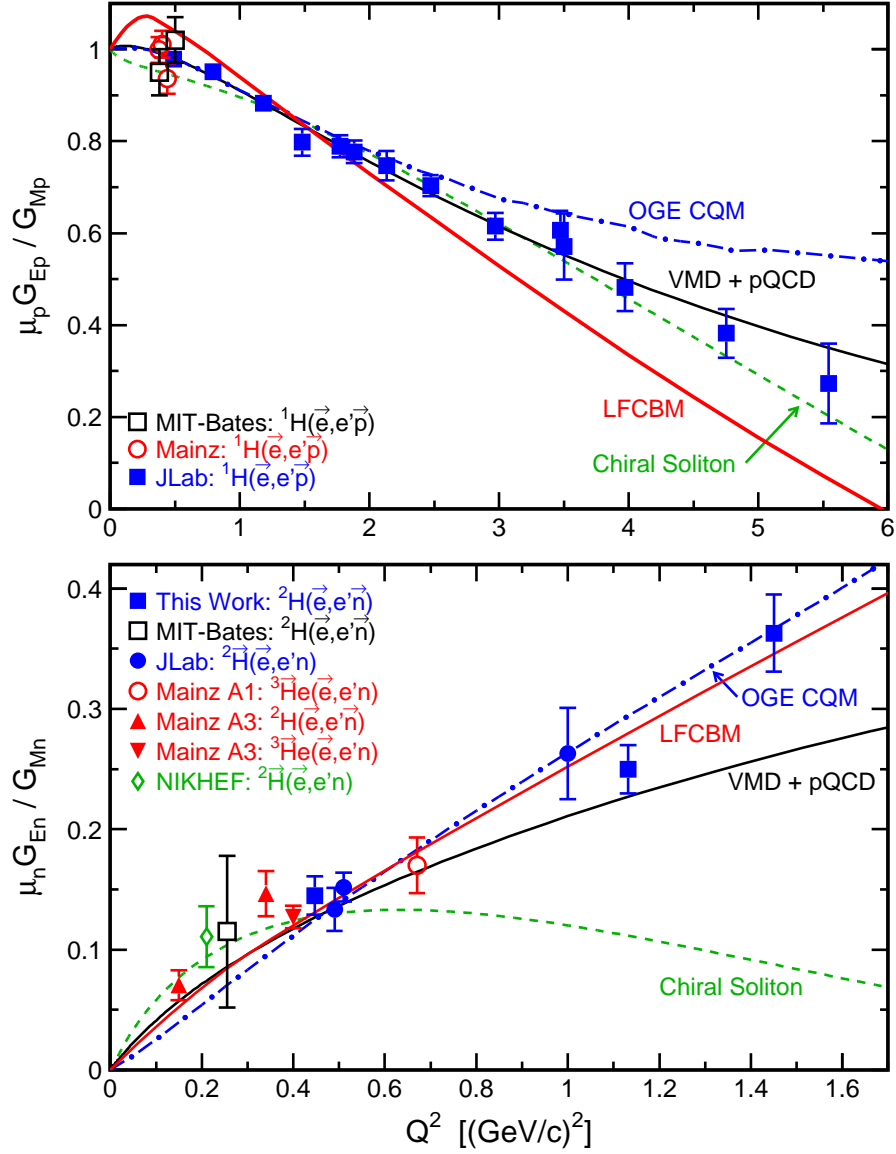


Figure 3: Predictions of selected models (see text for descriptions and the legend) for $\mu_p G_{Ep}^p / G_{Mp}^p$ and $\mu_n G_{En}^n / G_{Mn}^n$ compared with proton and neutron data. The neutron data symbols are the same as in Fig. 1.

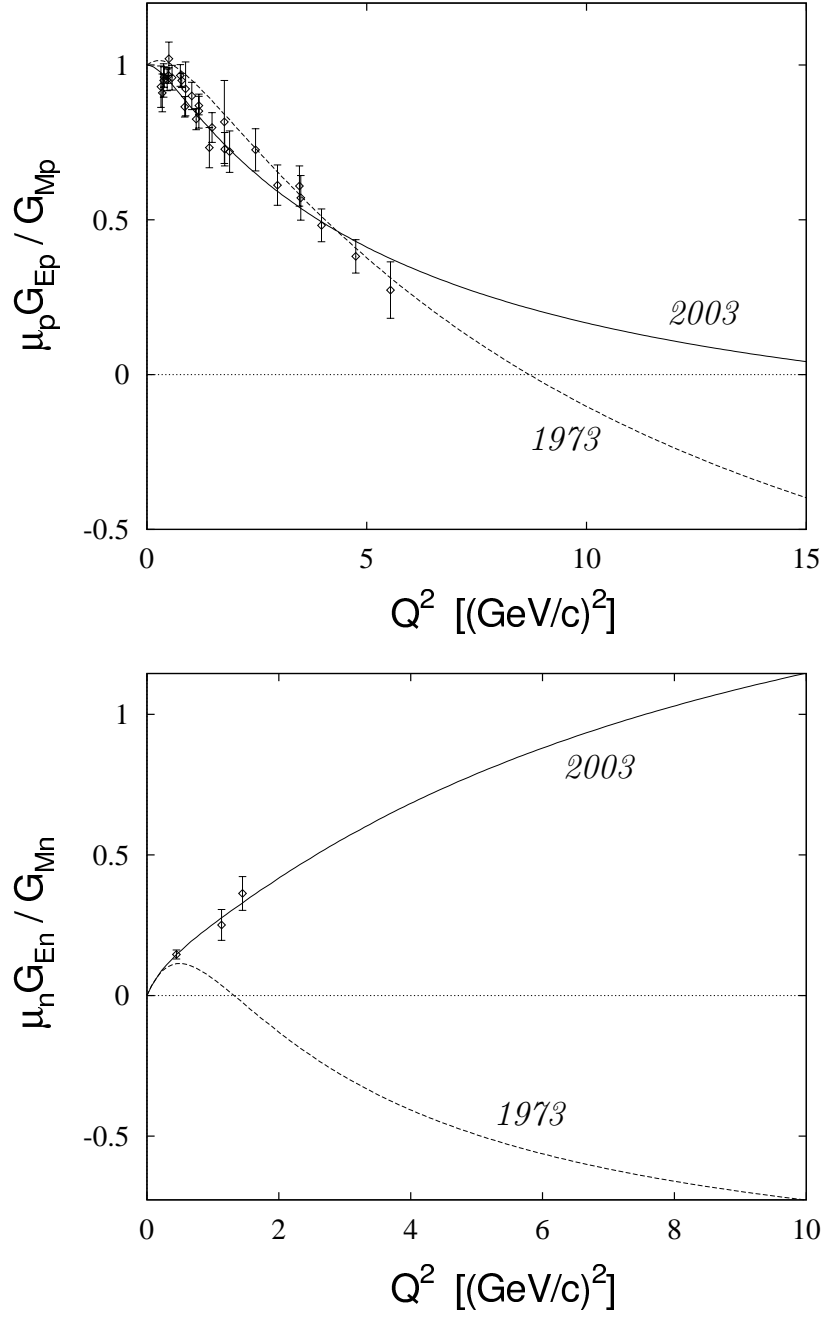


Figure 4: Predictions of the 1973 model (dashed) by Iachello, Jackson, and Lande, and the 2003 model (solid) by Bijker and Iachello for $\mu_p G_E^p / G_M^p$ (top panel) and $\mu_n G_E^n / G_M^n$ (bottom panel) compared with proton and neutron data.

the nucleon, the external photon couples to both the intrinsic structure and the meson cloud. Iachello [2003] showed that the 1973 model agrees well with the new Hall A data on the proton form factor ratio $\mu_p G_E^p/G_M^p$; however, this 1973 model disagrees with the JLab E93-038 data on the neutron form factor ratio $\mu_n G_E^n/G_M^n$. Very recently (after Iachello's September 2003 visit to JLab), Bijker and Iachello [2003] carried out a new isospin-invariant calculation that yielded agreement with the E93-038 neutron data. This 2003 calculation allows an intrinsic spin-flip amplitude, in addition to the spin-flip amplitude coming from the vector mesons. The results from both the 1973 and 2003 calculations are shown in Fig. 4 as a function of Q^2 ; the ratio for protons (neutrons) is shown in the top (bottom) panel. For G_E^p , the 1973 calculation predicts a zero at about 8 (GeV/c)², whereas the 2003 calculation pushes this zero to about 15 (GeV/c)²; for G_E^n , the 2003 calculation predicts a zero at Q^2 in excess of 20 (GeV/c)². To discriminate between various models, it is necessary to determine the Q^2 values where the zero crossings occur. The two calculations shown in Fig. 4 represent two limiting cases:

- (1) 1973 calculation: Helicity here is strictly conserved in the intrinsic part and the Pauli form factor F_2 comes entirely from coupling to the vector mesons.
- (2) 2003 calculation: Helicity flip is allowed in the intrinsic part (as in the light front calculations). The anomalous part of the form factor, F_2 , comes almost entirely from intrinsic spin-flip components (not from vector mesons).

At the moment, the proton data prefer the 1973 calculation because the 2003 calculation deviates from the proton data at high Q^2 . The neutron data need the 2003 calculation; the 1973 calculation deviates markedly from the E93-038 neutron data. Hence, measurements of the sign of G_E^p at 9-10 (GeV/c)² and G_E^n at 3-4 (GeV/c)² are crucial for disentangling the structure of the nucleon.

1.3 Better Understanding of Electron Scattering Data From Nuclei

In their paper on electron scattering from nuclei, Drechsel and Giannini (1989) state (on page 1109) that "*All calculations of nuclear electromagnetic properties suffer from the poor knowledge of G_E^n .*" As Q^2 increases, the values of G_E^p , the electric form factor of the proton, approach the values of G_E^n , represented by the modified Galster parameterization. Plotted in Fig. 5 (top panel) as a function of Q^2 are the neutron electric form factor for the modified Galster parameterization, the proton electric form factor for the dipole parameterization, and the proton electric form factor points measured in JLab E93-027. The measured G_E^p points have been fitted with the following parameterization:

$$G_E^p = G_D [1 - 0.14(Q^2 - 0.30)] \quad (\text{Fit to Hall A FPP Measurements}) \quad (4)$$

with

$$G_D \equiv (1 + Q^2/0.71)^{-2} \quad (\text{Dipole}) \quad (5)$$

The magnitude of G_E^n is not insignificant compared to G_E^p in the Q^2 region above about 2 (GeV/c)². The value of G_E^n from the modified Galster fit exceeds the value of G_E^p above $Q^2 \sim 4.5$ (GeV/c)². The ratio of G_E^p (E93-027) to G_E^n (modified Galster) is plotted in the bottom

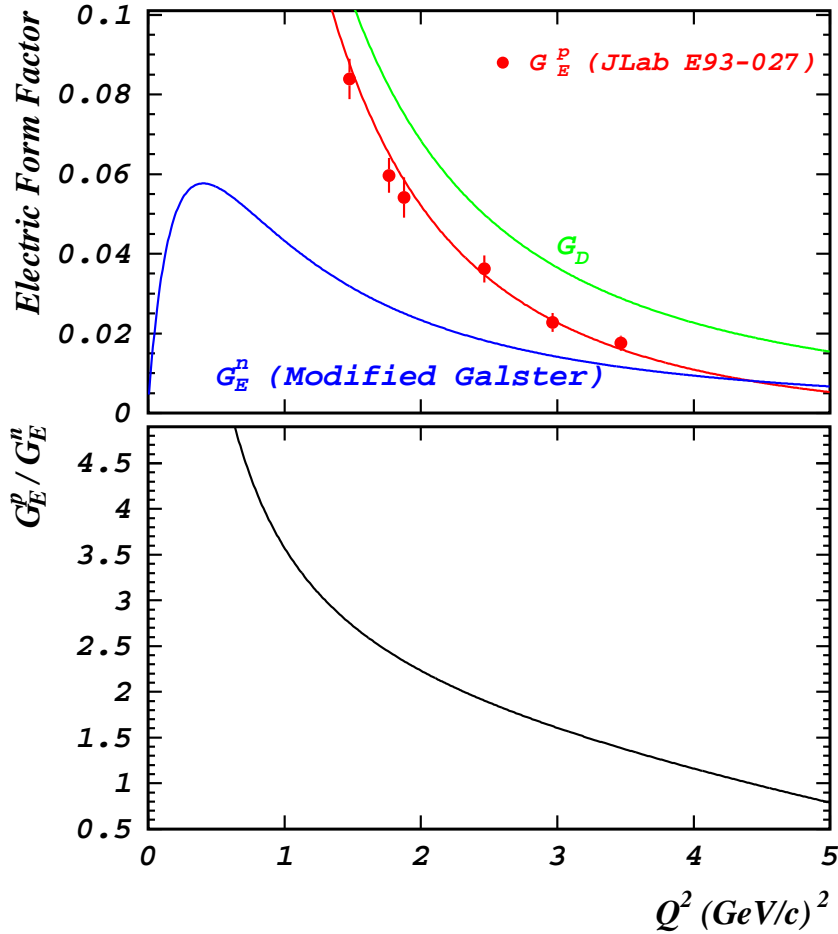


Figure 5: Proton and neutron form factors as a function of Q^2 . The red solid line in the top panel is a parameterization from Eq. (4) for G_E^p .

panel of Fig. 5. The G_E^p data measured in E93-027 turned out to be a surprise – falling faster with Q^2 than expected from the global analysis of earlier SLAC data. The nature of the decrease of G_E^n with Q^2 may be a surprise also.

Because the isovector electric form factors of nuclei are proportional to the difference $G_E^p - G_E^n$ (and the isoscalar electric form factors are proportional to the sum $G_E^p + G_E^n$), the value of G_E^n is needed for the understanding of electron scattering experiments that probe electric structure functions at high momentum transfer. The ratio of the isoscalar cross section to the isovector cross section depends sensitively on the value of G_E^n :

$$\frac{\sigma_{\text{isoscalar}}}{\sigma_{\text{isovector}}} = \left(\frac{G_E^p + G_E^n}{G_E^p - G_E^n} \right)^2 \quad (6)$$

This ratio is plotted in Fig. 6 as a function of Q^2 . This ratio is unity if $G_E^n = 0$; however, this ratio is about 18 at $Q^2 = 3.0$ (GeV/c)², and about 176 at $Q^2 = 4.0$ (GeV/c)² if G_E^n continues to follow the modified Galster parameterization and if G_E^p follows Eq. (4). A better knowledge of G_E^n is needed for the interpretation of electron scattering from nuclei at high momentum transfer. This knowledge is needed for the analysis of few-body data from measurements at

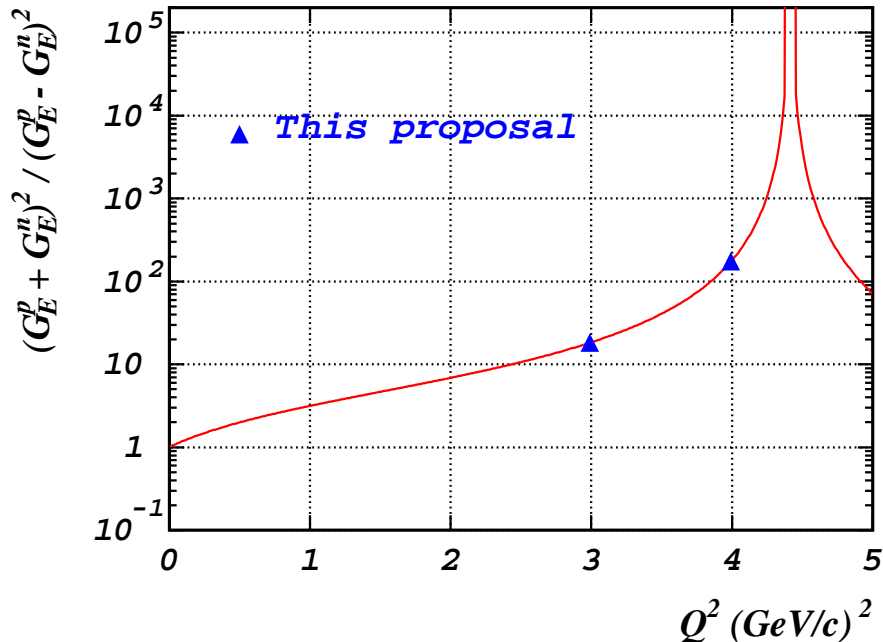


Figure 6: The ratio of isoscalar and isovector cross-sections [Eq. (6)] as a function of Q^2 . We assume the modified Galster parameterization for G_E^n and the parameterization from Eq. (4) for G_E^p .

Jefferson Lab, which are in the Q^2 range above the existing G_E^n data. With an uncertainty $\Delta G_E^n \approx 0.0032$, we will be able to distinguish easily between $G_E^n = 0$ and the modified Galster parameterization at the Q^2 values proposed herein.

1.4 Nuclear Physics Corrections and Reaction Mechanism Questions

Figure 7 shows the results from E93-038 for three cases: (1) The black triangles are for a point acceptance; (2) the red circles are acceptance-averaged PWBA values; and (3) the blue squares are the acceptance-averaged values based on Arenhoevel's full calculation [including FSI, MEC, and IC]. In E93-038, the nuclear physics corrections [for FSI, MEC, and IC] increased G_E^n over the values obtained with the PWBA by 5.6, 4.0, and 3.3 percent at $Q^2 = 0.45, 1.13,$ and 1.45 $(\text{GeV}/c)^2$, respectively. While the magnitude of the nuclear corrections are expected to continue to decrease with increasing Q^2 , the nuclear corrections are more reliable [and probably smaller] for deuterium than for helium. Arenhoevel [2003] is carrying out calculations for deuterium at our kinematics for $Q^2 = 3.0$ and 4.0 $(\text{GeV}/c)^2$.

Also, the reaction mechanism is expected to be simpler in deuterium than in helium. In the case of the proton form factor, reaction mechanism questions remain when comparing the Rosenbluth separation measurements with the recoil polarization measurements. Two or more independent measurements of the neutron are needed to alleviate questions about the reaction mechanism.

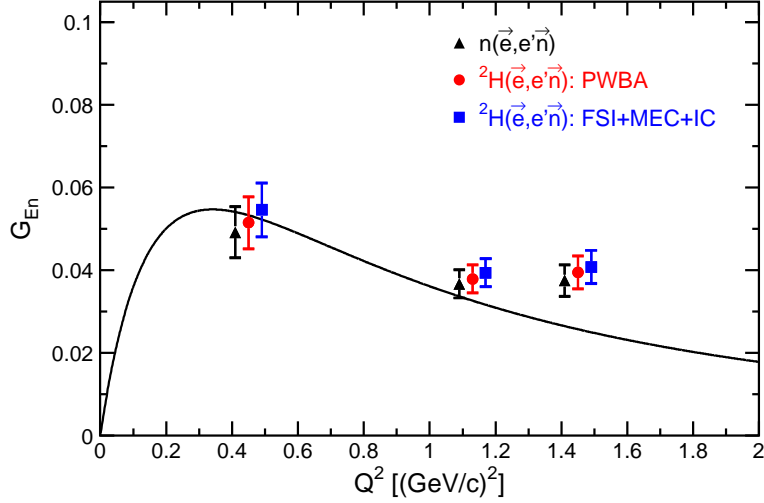


Figure 7: Comparison of the final results for G_{En}^n extracted from analyses assuming $n(\vec{e}, e'\vec{n})$ elastic scattering and a point acceptance (black triangles), the acceptance-averaged $^2\text{H}(\vec{e}, e'\vec{n})^1\text{H}$ Arenhövel PWBA model (red circles), and the acceptance-averaged $^2\text{H}(\vec{e}, e'\vec{n})^1\text{H}$ Arenhövel FSI+MEC+IC model (blue squares). The error bars shown are the quadrature sum of the statistical and systematic errors, and the solid curve is the Galster parameterization.

2 Theoretical Background

Arenhoevel (1987) calculated the effect of the electric form factor of the neutron on the polarization transfer in the $d(\vec{e}, e'\vec{n})p$ reaction in the quasifree region, where the deuteron serves as a neutron target while the proton acts mainly as a spectator. Using a nonrelativistic theory and a realistic nucleon-nucleon potential, Arenhoevel found that the sideways polarization of the recoil neutron $P_{S'}$, which vanishes for coplanar kinematics and unpolarized electrons, is most sensitive to G_E^n for neutron emission along the momentum-transfer direction in the quasifree case. Using the parameterization of Galster et al. (1971) for G_E^n , Arenhoevel's calculation indicates that even away from the forward-emission direction (with respect to the direction of the momentum transfer \vec{q}), the increase in the sideways polarization of the neutron $P_{S'}$ is small for $G_E^n = 0$, but increases when G_E^n is switched on, and that this increase prevails up to a neutron angle of nearly 30° measured with respect to $\vec{q}^{c.m.}$ in the center-of-mass system. In the forward direction with respect to $\vec{q}^{c.m.}$, Arenhoevel found also that the neutron polarization $P_{S'}$ is insensitive to the influence of final-state interactions (FSI), meson-exchange currents, and isobar configurations, and that this lack of sensitivity holds again up to an angle of nearly 20° away from the forward direction with respect to $\vec{q}^{c.m.}$, which corresponds to a laboratory angle of about a few degrees away from the forward direction with respect to the \vec{q}^{lab} . Arenhoevel also studied the influence of different deuteron wave functions on the sideways neutron polarization $P_{S'}$. His results for quasifree kinematics (i.e., for neutron emission along \vec{q}) show almost no dependence on the deuteron model. The Arenhoevel calculation shows that dynamical uncertainties are very small. Finally, Beck and Arenhoevel (1992) investigated the role of relativistic effects in electrodisintegration of the deuteron for quasifree kinematics. They found that the dependence on the parameterization of the nucleon current in terms of Dirac-Pauli or Sachs form factors is reduced considerably by inclusion of the relativistic contributions. Also, for quasifree emission,

Arenhoevel (2002) demonstrated that P_L is insensitive to FSI, MEC, IC, and to theoretical models of deuteron structure.

Rekalo, Gakh, and Rekalo (1989) used the relativistic impulse approximation to describe the polarization effects sensitive to G_E^n in deuteron electrodisintegration. In the deuteron quasielastic peak, the neutron polarizations calculated in the relativistic approach agree with the results of Arenhoevel (1987). A later study by Mosconi, Pauschenwein, and Ricci (1991) of nucleonic and pionic relativistic corrections in deuteron electrodisintegration does not change the results of Arenhoevel. Laget (1990) investigated the effects of nucleon rescatterings and meson-exchange currents on the determination of the neutron electric form factor in the $d(\vec{e}, e'\vec{n})p$ reaction. He concluded that the measurements of the sideways polarization of the neutron appears to be the most direct way to determine the neutron electric form factor. He concluded also that in quasifree (colinear) kinematics, the neutron polarization in the exclusive reaction is equal to the value expected in the elementary reaction $n(\vec{e}, e'\vec{n})$ and that corrections from final-state interactions and meson-exchange currents are negligible above $Q^2 = 0.30$ (GeV/c)², but that these corrections become sizeable below this momentum transfer; however, Herberg et al. (1999) found that (even in the quasifree peak) corrections for FSI in $d(\vec{e}, e'\vec{n})p$ measurements at Mainz amounted to $(8\pm 3)\%$ for $Q^2 = 0.34$ (GeV/c)² and $(65\pm 3)\%$ for $Q^2 = 0.15$ (GeV/c)² of the value unperturbed by FSI. In E93-038, we found that the nuclear physics [FSI+MEC+IC] corrections were small and decreased with increasing Q^2 . The nuclear physics corrections increased G_E^n over the value obtained with the PWBA by only 5.6, 4.0, and 3.3 percent at $Q^2 = 0.45, 1.13,$ and 1.45 (GeV/c)², respectively. These corrections were based on the model of Arenhoevel et al. (1988).

3 Description of the Experiment

3.1 Experimental Arrangement

The experimental arrangement is similar to the one used in E93-038 (shown in Fig. 8). A polarimeter detects the recoil neutron from the quasielastic $d(\vec{e}, e'\vec{n})p$ reaction and measures the up-down scattering asymmetry from the projection of the polarization vector on the transverse axis. A dipole magnet (CHARYBDIS) in front of the polarimeter precesses the neutron polarization vector through an angle χ to permit measuring the scattering asymmetry ξ_+ from the polarization vector component on the transverse (or sideways) direction. With another measurement of the scattering asymmetry ξ_- for a precession through an angle $-\chi$, the ratio of G_E and G_M is given by

$$g \equiv \left(\frac{G_E}{G_M} \right) = K_R \tan(\chi) \frac{(\eta + 1)}{(\eta - 1)} \quad (7)$$

where the asymmetry ratio

$$\eta \equiv \frac{\xi_-}{\xi_+} = \frac{P_-^x}{P_+^x} \quad (8)$$

and K_R is a kinematic function that is determined by the electron scattering angle θ_e in the $d(\vec{e}, e'\vec{n})p$ reaction. For a total data-acquisition time T , the time fractions for measuring ξ_+ and ξ_- are optimized to minimize the statistical uncertainty in g . The scattered electron from the $d(\vec{e}, e'\vec{n})p$ reaction is detected with the high-momentum spectrometer (HMS) in coincidence with the recoil neutron.

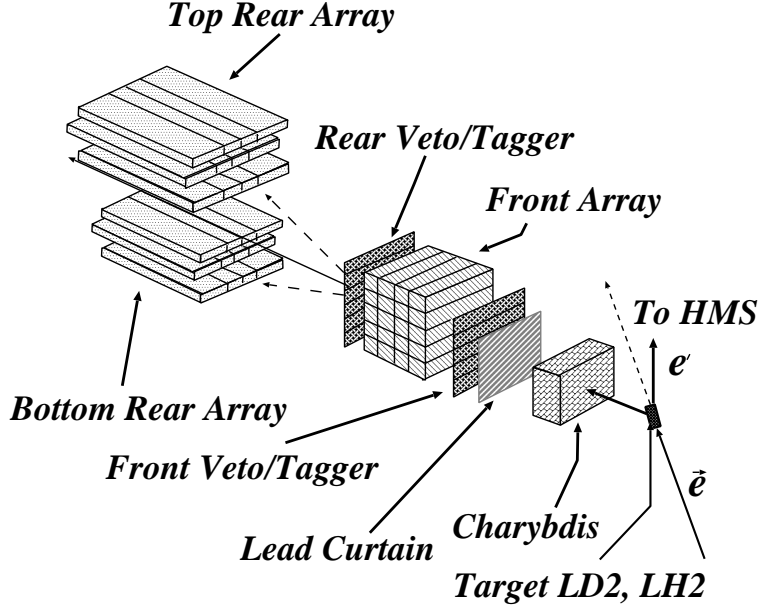


Figure 8: Schematic diagram of the experimental arrangement in E93-038.

The polarimeter to be used for these measurements (see Fig. 9) is an enhanced version of the one used for E93-038. In order to increase the efficiency, we are increasing the number of detector layers in the front array to six layers [from the four used in E93-038], and we are inserting steel converters ahead of each layer in the rear detector arrays [Semenova et al. (2002)]. Also, we optimize the geometry so that the mean scattering angle is at the peak of the analyzing power. The polarimeter now consists of 30 detectors in the front array and 18 detectors in each of two rear arrays for a total of 66 detectors. A double layer of veto/tagger detectors is located ahead of the front array, and another double layer of tagger detectors is located behind the front array. To permit high luminosity, the dimensions of each of the 30 detectors in the front array are 10 cm×10 cm×100 cm, and the 18 [10 in×40 in×4 in] detectors in each rear array are shielded from the direct path of neutrons from the target.

A significant advantage of this technique for measuring the ratio of the two scattering asymmetries is that the scale and systematic uncertainties are minimal because the relative uncertainty in the analyzing power of the polarimeter does not enter in the ratio. The same is true for the beam polarization P_L because, as demonstrated in E93-038, P_L does not change much during sequential measurements of ξ_+ and ξ_- .

In the cross-ratio method of analysis of the scattering asymmetries measured in the polarimeter, Ohlsen and Keaton (1973) showed that false asymmetries cancel to all orders from helicity-dependent errors in charge integration or system dead-times, or from errors in detection efficiency and acceptances; and that false asymmetries cancel to first order from misalignments with respect to \vec{q} , or from a difference in the beam polarization for the two helicity states. The cross ratio is the ratio of two geometric means $(N_U^+ N_D^-)^{1/2}$ and $(N_U^- N_D^+)^{1/2}$, where $N_U^+(N_D^-)$ is the yield in the peak for scattering neutrons up (down) when the helicity is positive (negative).

The systematic and scale uncertainties achieved in E93-038 are listed in Table I of Appendix A. The overall systematic uncertainties are of the order of 2%.

In E93-038, we used the CHARYBDIS dipole magnet with an 8.25-inch gap and 2-inch

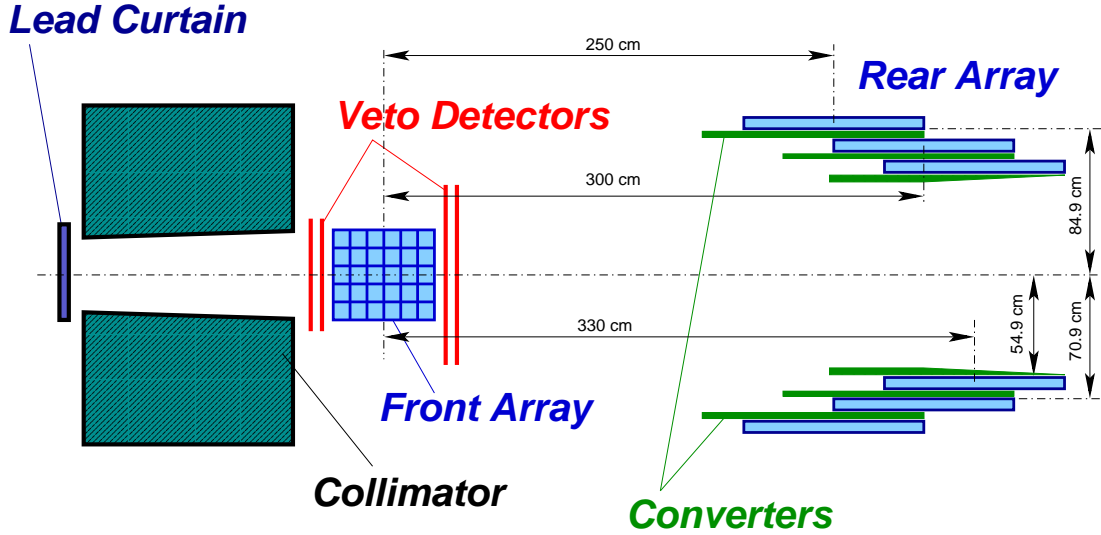


Figure 9: Neutron polarimeter to be used in the measurements.

field clamps. The 8.25-inch gap is large enough to illuminate fully the front detector of our polarimeter (20-inch high by 40-inch wide). The precession angle χ is the angle of rotation of the polarization vector measured with respect to the direction of motion of the particle in the rest frame of the particle after traversing the magnetic field. The neutron spin precession angle χ is given by

$$\chi = -\frac{ge}{2M_p c \beta_n} \int B \Delta l = \frac{1.913e}{M_p c \beta_n} \int B \Delta l \quad (9)$$

where $g/2 = -1.913$. The maximum central $\int B \Delta l = 2.39$ Tm for CHARYBDIS with an 8.25-inch gap.

The lead curtain ahead of the polarimeter is required to attenuate electromagnetic radiation and also to reduce the flux of charged particles incident on the polarimeter. The singles counting rate in one of the detectors decreases markedly when the thickness of the Pb increases from 5 cm to 10 cm; for example, the singles rates in one of the veto detectors (160 cm wide \times 11 cm high \times 0.64 cm thick) at a distance of about 6.7 m from a 15-cm LD₂ target are plotted in Fig. 10 as a function of the electron beam current at an energy of 884 MeV. For all beam currents, the singles rate is about five times higher with 5-cm Pb curtain. E93-038 used a 10-cm lead curtain in order to run at higher beam currents. We do not have data with a 5-cm lead curtain at higher beam energies. E93-038 ran with a 10-cm Pb curtain for all these energies. To measure the false asymmetry or the dilution of the asymmetry from the two-step process $d(\vec{e}, e'\vec{p})n + Pb(\vec{p}, \vec{n})$ we acquire data with an LH₂ target. In the second charge-exchange step, the sign of the polarization transferred to the neutron will be opposite to that from the primary $d(\vec{e}, e'\vec{n})p$ process because the sign of the magnetic moment of the proton is opposite that of the neutron. This effect increases as the $p - n$ charge exchange cross section increases in going to low Q^2 .

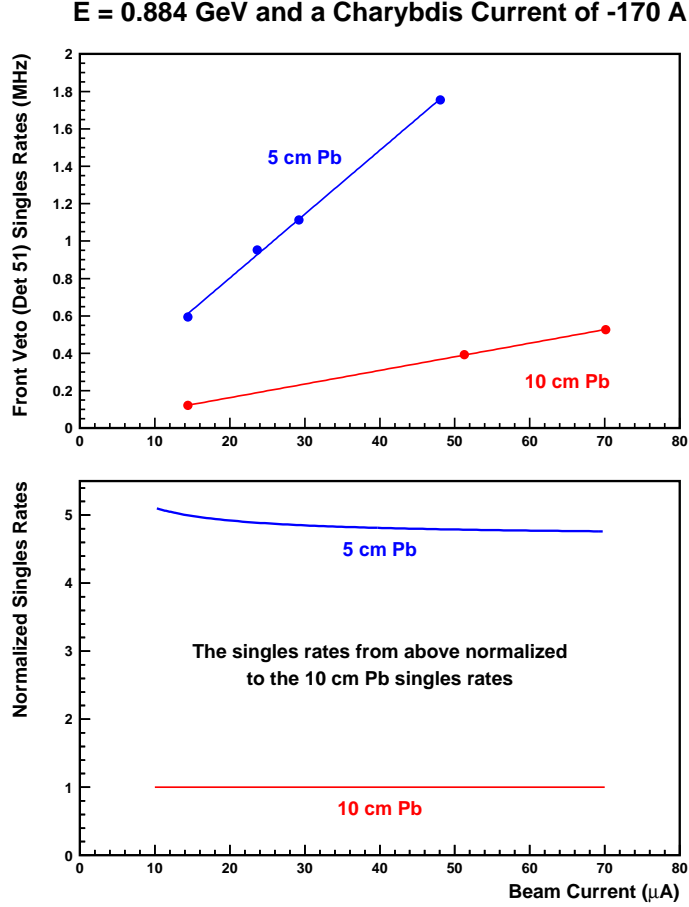


Figure 10: Singles rates for beam energy of 884 MeV and a CHARYBDIS current of -170 A.

3.2 Kinematics

Table 1 lists the kinematic conditions and the $B\Delta l$ required to precess the neutron polarization vector through χ degrees. The maximum beam energy was selected to be below 5.7 GeV where the accelerator operates reliably (with fewer trips of the cavities). The accelerator should be able to deliver a beam polarization of 80% at any energy (see Fig. 22). The range of reasonable angles of neutron spin precession is limited on the small-angle side by the requirement to have the magnetic field in CHARYBDIS strong enough to deflect a significant part of the quasielastic protons away from the front array of the polarimeter, and on the large-angle side by the fact that the statistical uncertainty increases with precession angle χ , as shown in Fig. 15. A precession angle χ of 20 (30) deg. was chosen for $Q^2 = 3.0$ (4.0) $(\text{GeV}/c)^2$. Smaller precession angles were avoided because the smaller Charybdis current would reduce the deflection of protons away from the front array.

3.3 Count Rates

The rate of electron-neutron coincidence events, which comes from quasielastic scattering of electrons on the 15-cm LD_2 target, was projected at $Q^2 = 3.0$ (4.0) $(\text{GeV}/c)^2$ for a beam current of 75 (55) μA (which corresponds to a beam luminosity $L = 3.58$ (2.62) $\times 10^{38} \text{ cm}^{-2}\text{s}^{-1}$). The

Four-Momentum Transfer, Q^2 (GeV/c) ²	3.0	4.0
Beam Energy, E_0 (GeV)	3.682	5.612
Electron Scattering Angle, θ_e (deg)	36.47	26.17
Scattered Electron Momentum, P_e (GeV/c)	2.080	3.476
Neutron Scattering Angle, θ_n (deg)	31.6	31.6
Neutron Momentum, P_n (GeV/c)	2.359	2.926
Neutron Kinetic Energy, T_n (MeV)	1600	2134
Neutron Velocity, β_n	0.929	0.952
Flight Path, x (m)	7.0	7.0
Precession Angle, χ (deg)	20	30
Field Integral to Precess Neutron Spin through χ Degree, $B\Delta l$ (Tm)	0.5309	0.8161
CHARYBDIS Current, I (A)	131.3	201.7

Table 1: Kinematic conditions at a neutron scattering angle of 31.6°. Also listed is the Charybdis field integral $B\Delta l$ required to precess the neutron polarization vector.

calculation was done for a momentum bite $\Delta p/p$ of $-3/+5\%$ for the scattered electron. The restricted HMS momentum bite (combined with the cuts on the missing momentum and HMS-NPOL coincidence time) helps to suppress the neutrons associated with pion production (see Fig. 16).

The acceptances for E93-038 were calculated for the HMS in the normal-quad mode and in the rear position. We used the kinematic conditions from Table 1 for two Q^2 -points of 3.0 and 4.0 (GeV/c)². Based on the acceptance-averaged HMS-NPOL coincidence rate of quasielastic events, $\langle R_{MCEEP} \rangle$, from MCEEP [Ulmer (1991) version 3.6 includes radiative corrections], we estimated the real-event rate R_{real} for an HMS efficiency $\epsilon_{HMS} = 0.92$ [which is the product of a single-hit fraction in the wire chambers (0.95) and an efficiency for tracking a good electron (0.97)], the HMS momentum bite of $-3/+5\%$, and the HMS-NPOL coincidence time-of-flight ($cTOF$) window of ± 1 ns. For this estimation, we simulated the neutron polarimeter efficiency, ϵ_n , (including neutron transmission through 10-cm lead curtain and lost of events due to analysis cuts) and the polarimeter analyzing power, A_Y , with the FLUKA 2002 code (see also Section 4 and Fig. 21). Listed in Table 2 are neutron polarimeter and HMS acceptances, estimated neutron polarimeter parameters (viz., A_Y and ϵ_n), and the calculated real event rate.

3.4 Projected Uncertainties

The up-down asymmetry, measured in JLab E93-038, is proportional to the projection of the neutron polarization vector on the axis that is perpendicular to the neutron momentum direction. Thus, the ratio of asymmetries for neutron spin precession through $\pm\chi$ degrees is given by:

$$\eta \equiv \frac{\xi_-}{\xi_+} = \frac{P_-^x}{P_+^x} = \frac{P_{S'} \cos(-\chi) + P_{L'} \sin(-\chi)}{P_{S'} \cos(\chi) + P_{L'} \sin(\chi)} = \frac{(P_{S'}/P_{L'}) \cos(\chi) - \sin(\chi)}{(P_{S'}/P_{L'}) \cos(\chi) + \sin(\chi)} \quad (10)$$

$$(P_{S'}/P_{L'}) = \frac{-\sin(\chi) (\eta + 1)}{\cos(\chi) (\eta - 1)} = -\tan(\chi) \frac{(\eta + 1)}{(\eta - 1)} \quad (11)$$

Four-Momentum Transfer, Q^2 (GeV/c) ²	3.0	4.0
HMS angular acceptance:		
$\Delta\theta_e$ (mrad)	± 27.5	± 27.5
$\Delta\phi_e$ (mrad)	± 71.9	± 71.9
HMS efficiency, ϵ_e (%)	92.0	92.0
Neutron polarimeter angular acceptance:		
$\Delta\theta_n$ (mrad)	± 71.4	± 71.4
$\Delta\phi_n$ (mrad)	± 35.7	± 35.7
Neutron polarimeter efficiency, ϵ_n (%)	1.0	1.0
Beam Current, I_{beam} (μ A)	75	55
MCEEP rate, $\langle R_{MCEEP} \rangle$ (Hz)	51.7	23.4
Real-event rate, R_{real} (Hz)	0.47	0.22
Neutron polarimeter analyzing power, A_Y	0.09	0.07
Precession Angle, χ (deg)	20	30
Expected asymmetries:		
for $-\chi$ precession (%)	-0.8	-1.1
for $+\chi$ precession (%)	2.6	2.1

Table 2: The neutron polarimeter and HMS acceptances, estimated neutron polarimeter parameters, and calculated real event rate at $Q^2 = 3.0$ and 4.0 (GeV/c)² for a beam current of 75 and 55 μ A, respectively, incident on a 15-cm LD_2 target. Also listed are the simulated NPOL efficiency and analyzing power (see Section 4 and Fig. 21 for details), and expected asymmetries for $-\chi$ and $+\chi$ precession of the neutron polarization vector.

where $P_{S'}$ and $P_{L'}$ are transverse and longitudinal projections of the neutron polarization vector:

$$P_{S'} = -h P_e \frac{K_S g}{K_0 (1 + g^2/K_0)} \quad (12)$$

$$P_{L'} = h P_e \frac{K_L}{K_0 (1 + g^2/K_0)} \quad (13)$$

Here h is the beam helicity, P_e is the beam polarization, and $g \equiv (G_E/G_M)$.

$$(P_{S'}/P_{L'}) = -g (K_S/K_L) \quad (14)$$

From (14) and (11) :

$$g = -\left(\frac{K_L}{K_S}\right) \left(\frac{P_{S'}}{P_{L'}}\right) = \left(\frac{K_L}{K_S}\right) \tan(\chi) \frac{(\eta + 1)}{(\eta - 1)} \quad (15)$$

The statistical uncertainty in the g value is:

$$(\delta g)_{stat} = \left(\frac{K_L}{K_S}\right) \tan(\chi) \frac{2}{(\eta - 1)^2} \delta\eta \quad (16)$$

The relative statistical uncertainty $(\delta g/g)_{stat}$ is:

$$\left(\frac{\delta g}{g}\right)_{stat} = \frac{2}{(\eta + 1)(\eta - 1)} \delta\eta \quad (17)$$

Flux at 31.6° behind 10.16-cm Pb; E=3682 MeV; 15-cm LD₂

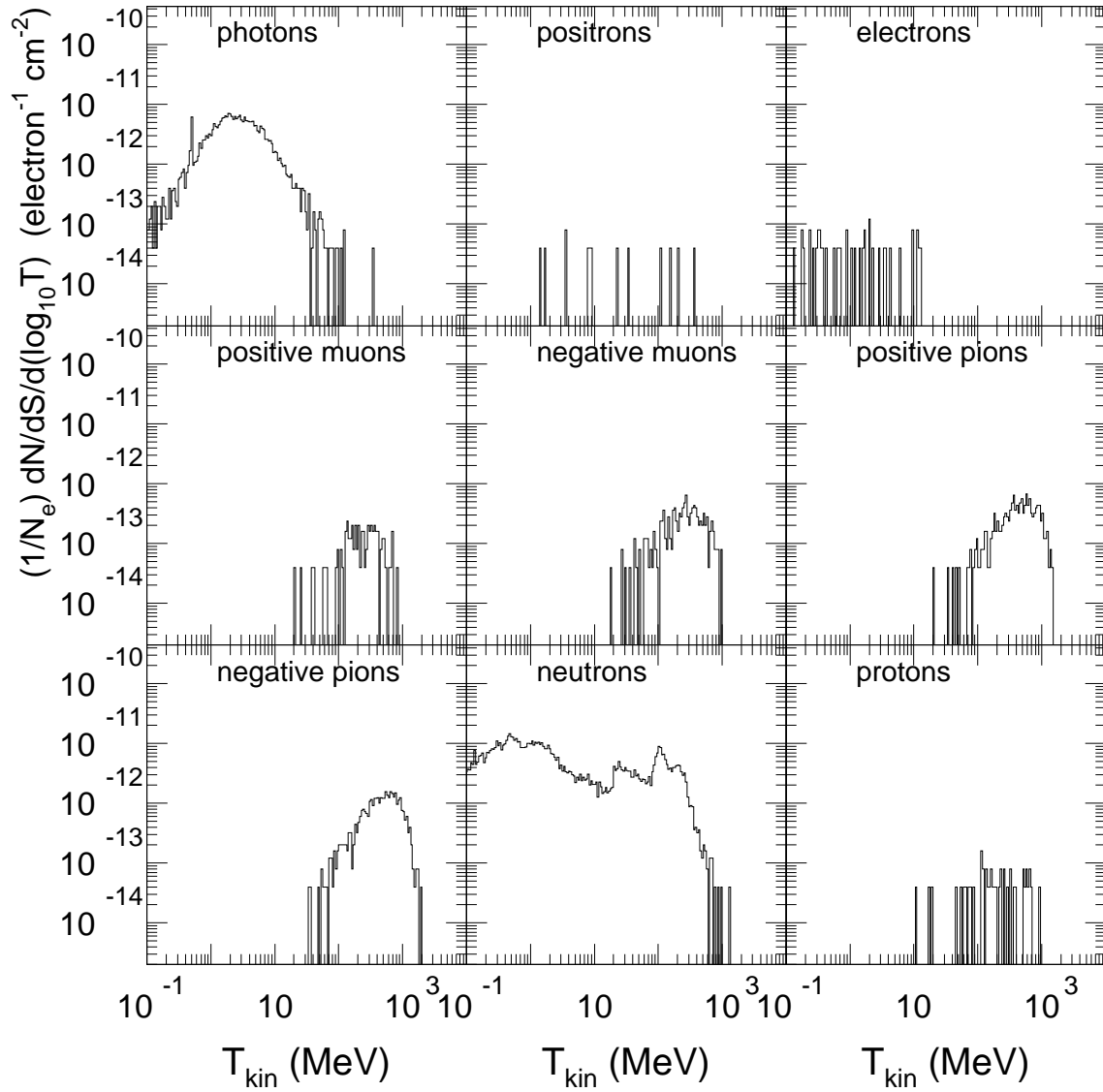


Figure 11: Simulated spectra of the particles at 31.6° behind 4-in Pb curtain from 3.682 GeV electron beam incident on a 15-cm LD₂ target.

Flux at 31.6° behind 10.16-cm Pb; E=5612 MeV; 15-cm LD₂

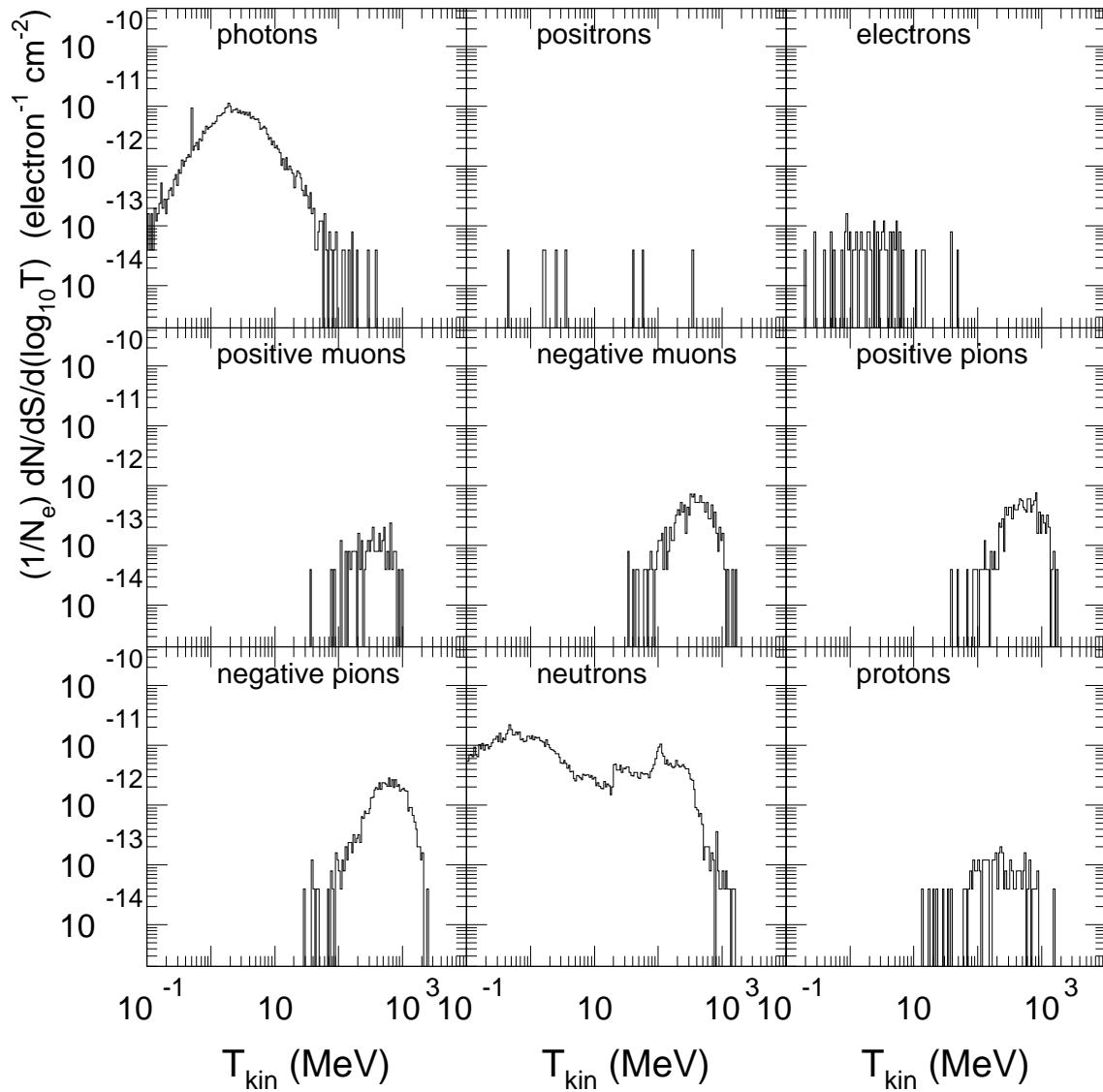


Figure 12: Simulated spectra of the particles at 31.6° behind 4-in Pb curtain from 5.612 GeV electron beam incident on a 15-cm LD₂ target.

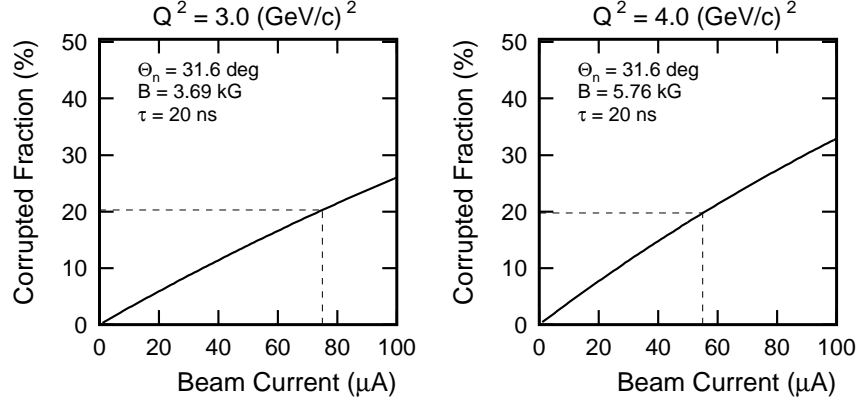


Figure 13: Calculated fraction of electron-neutron coincidence events corrupted from a background particle (charged or neutral) that appears during the coincidence time window of 20 ns as a function of the beam current.

Here $\delta\eta$ is the statistical error in the asymmetry ratio:

$$\left(\frac{\delta\eta}{\eta}\right)^2 = \left(\frac{\delta\xi_-}{\xi_-}\right)^2 + \left(\frac{\delta\xi_+}{\xi_+}\right)^2 \quad (18)$$

or

$$(\delta\eta)^2 = \left(\frac{\delta\xi_-}{\xi_+}\right)^2 + \xi_-^2 \left(\frac{\delta\xi_+}{\xi_+^2}\right)^2 \quad (19)$$

To project the statistical uncertainties, we used the statistical errors for asymmetries which come from Poisson statistics:

$$\left(\frac{\delta\xi_{\pm}}{\xi_{\pm}}\right)^2 = \frac{1}{\xi_{\pm}^2} \left(\frac{1+2/r}{N_{\pm}}\right) = \frac{1}{(A_Y P_{\pm}^x)^2} \left(\frac{1+2/r}{N_{\pm}}\right) \quad (20)$$

Here N_{\pm} is the number of events taken during $\pm\chi$ precession angle runs, A_Y is the polarimeter analyzing power, and r is the ratio of real-to-accidental coincidences. For these projections, we used the value $r = 26$ (21) from the simulation for $Q^2 = 3.0$ (4.0) $(\text{GeV}/c)^2$. The accidental coincidence rates were calculated with a combination of the MONQEE code (Dytman 1987) for the electron single rates in the HMS and the program of P. Degtyarenko to calculate the neutron single rates in the polarimeter. This program, based on GEANT 3.21 (Brun 1993), uses the GCALOR (Zeitnitz 1994) program package in order to simulate hadronic interactions down to 1 MeV for nucleons and charged pions and into the thermal region for neutrons, and uses DINREG (Degtyarenko 1992, 2000) – Deep Inelastic Nuclear Reaction Exclusive Generator with a model for hadronic interactions of electrons and photons. Values of r achieved in E93-038 are compared with the results of simulation in Fig. 20. Using the single rates of neutral and charged particles in the polarimeter from the simulation with the program of P. Degtyarenko (see Figs. 11, 12), we calculated a fraction of electron-neutron coincidence events corrupted from a background particle (charged or neutral) that appears during a coincidence time window of 20 ns. For a 75 (55) μA beam at $Q^2 = 3.0$ (4.0) $(\text{GeV}/c)^2$, the corrupted fraction is calculated to be about 20% (see Fig. 13).

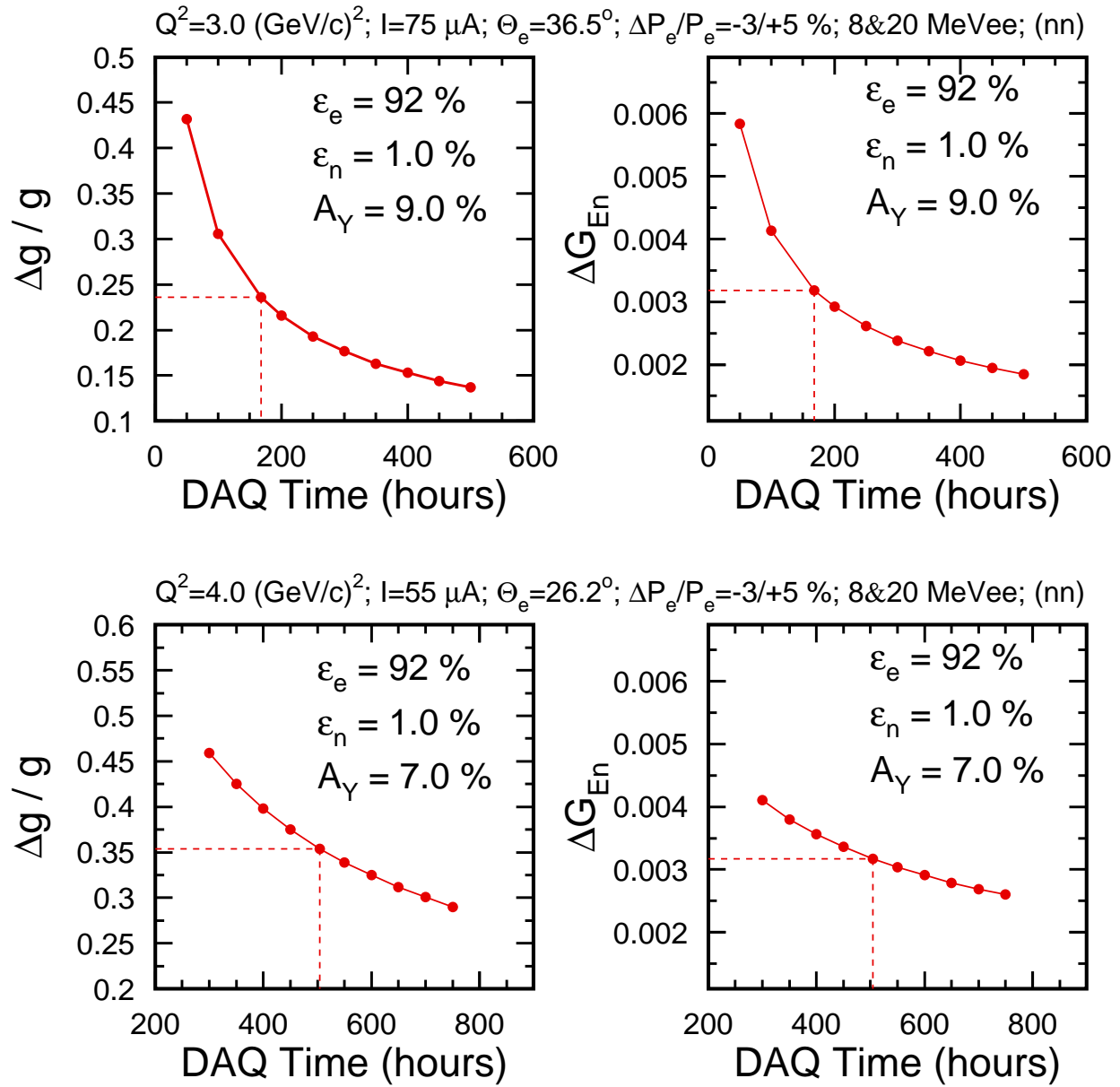


Figure 14: Top (bottom) panels: Projected uncertainties $\Delta g_n/g_n$ and ΔG_E^n at $Q^2 = 3.0$ (4.0) $(\text{GeV}/c)^2$ as a function of the DAQ time for a beam current of 75 (55) μA .

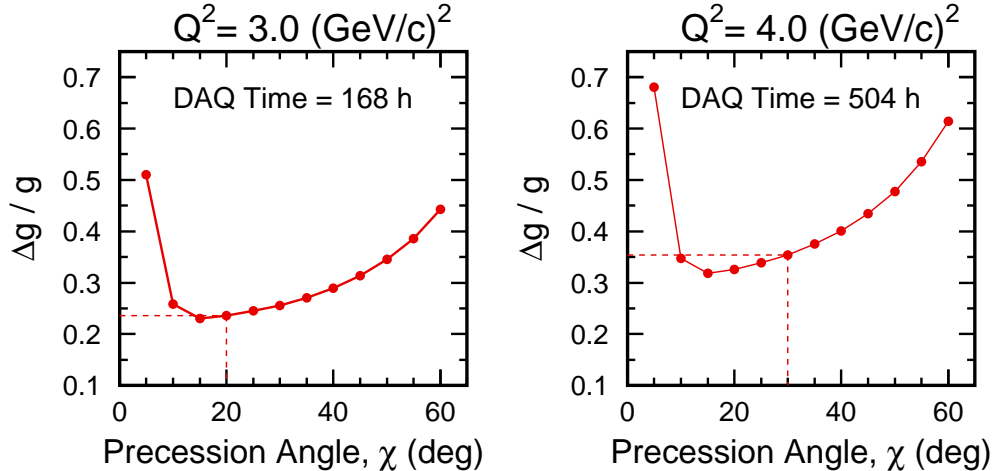


Figure 15: Statistical uncertainty $\Delta g/g$, projected at $Q^2 = 3.0$ and 4.0 $(\text{GeV}/c)^2$, as a function of precession angle χ .

The projected uncertainties $\Delta g_n/g_n$ and ΔG_E^n are plotted in Fig. 14 as a function of the data acquisition time at $Q^2 = 3.0$ (4.0) $(\text{GeV}/c)^2$ for a luminosity of 3.58 (2.62) $\times 10^{38}$ $\text{cm}^{-2}\text{s}^{-1}$, which is achievable with a beam current of 75 (55) μA on a 15-cm liquid deuterium target. The DAQ time that is designated by the dotted line in Fig. 14 was chosen to target an uncertainty ΔG_E^n in the vicinity of 0.0032.

Figure 15 shows the statistical uncertainty $\Delta g/g$, projected at $Q^2 = 3.0$ and 4.0 $(\text{GeV}/c)^2$ for the DAQ time of 168 and 504 hours, respectively, as a function of precession angle χ .

4 Some Results from E93-038

The purpose of this section is to indicate the quality of the data obtained and the simulation made in E93-038. We selected real quasielastic ${}^2\text{H}(\vec{e}, e'n)$ events using a restricted HMS momentum bite, the cut on the missing momentum, and the cut on HMS-NPOL coincidence time (see Fig. 16). Typical time-of-flight spectra for the highest Q^2 [viz., $Q^2 = 1.45$ $(\text{GeV}/c)^2$] are shown in Fig. 17. The left panel is an HMS-NPOL coincidence time-of-flight spectrum. We compared the measured time-of-flight, cTOF, with the time-of-flight calculated from electron kinematics and offsets determined by a calibration procedure; the result is centered on zero with a FWHM of approximately 1.5 ns, and the reals-to-accidentals ratio is ≈ 12 at a beam current of ≈ 50 μA [see Fig. 20]. The right panel is the time-of-flight spectrum between a neutron event in the front array and an event in the top or bottom rear array. We compared this measured time-of-flight, ΔTOF , with the time-of-flight calculated for elastic np scattering. This result, normalized to the nominal 2.5 m flight path, has a peak at zero also. The tail on the slow side is due to scattering from carbon, and the secondary peak at ~ -2.5 ns is the result of π^0 production in the front array. To extract the physical scattering asymmetry, we calculated the cross ratio, r , which is defined to be the ratio of two geometric means, $(N_U^+ N_D^-)^{1/2}$ and $(N_U^- N_D^+)^{1/2}$, where $N_U^+(N_D^-)$ is the yield in the ΔTOF peak for neutrons scattered up(down) when the beam helicity

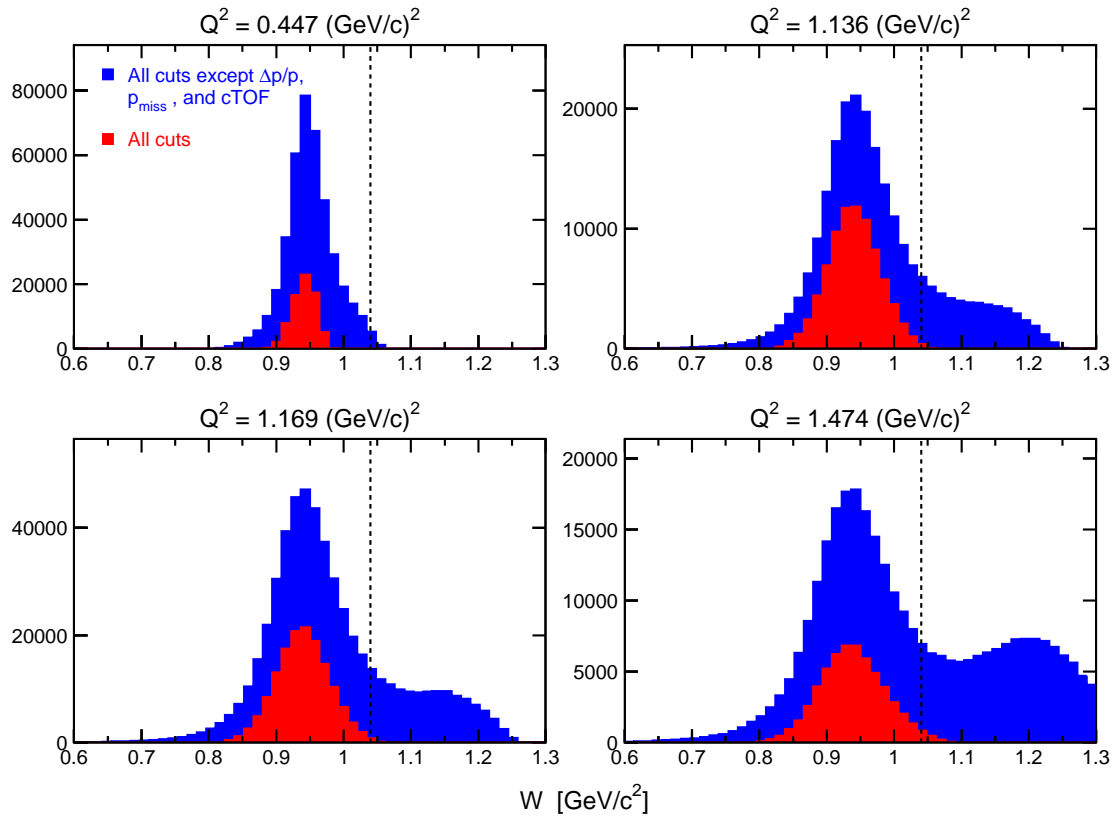


Figure 16: Invariant mass spectra before and after cuts on the scattered electron momentum, the missing momentum, and an HMS-NPOL coincidence time-of-flight.

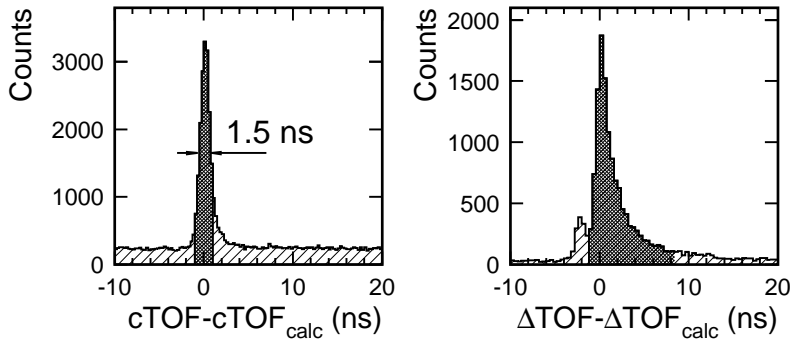


Figure 17: Typical time-of-flight spectra for $Q^2 = 1.45 \text{ (GeV/c)}^2$. Selected portions are shaded.

was positive(negative); the yields, corrected for background, were obtained by peak fitting. The physical scattering asymmetry is then given by $(r - 1)/(r + 1)$. The merit of the cross ratio technique [Ohlsen (1973)] is that the neutron polarimeter results are independent of the luminosities for positive and negative helicities, and the efficiencies and acceptances of the top and bottom halves of the polarimeter. Beam charge asymmetries (of typically 0.1%) and detector threshold differences cancel in the cross ratio. The result of an analysis of the asymmetries for each run at $Q^2 = 1.13 \text{ (GeV/c)}^2$ and the error-bar weighted average for these data appear in Fig. 18; the sign of the asymmetries from runs with the $\lambda/2$ -plate IN have been reversed. A histogram of the asymmetries (see Fig. 19) clearly demonstrates that the distribution of the asymmetries is of an appropriate Gaussian shape.

To estimate reals-to-accidentals ratio r , we simulated the rate of inclusive electrons in HMS with MONQUEE code [Dytman (1987)], and we used single rates in NPOL simulated with the GEANT-based program of P. Degtyarenko (for details, see Section 3.4). Simulated accidental coincidence rates and r -values are shown in Fig. 20 together with ones measured in E93-038. The large difference between the measured and calculated accidentals and the ratios of real-to-accidental coincidences at $Q^2 = 0.45 \text{ (GeV/c)}^2$ is because the calculation doesn't take into account the larger radiation background in Hall C caused by multiple scattering of electrons at this lowest beam energy of 884 MeV.

We simulated the E93-038 neutron polarimeter efficiency, ϵ_n , (including a neutron transmission through 10-cm lead curtain) using the FLUKA-2002 program, version 2.0 [Fasso et al. (2001)]. The “stand-alone” (not GEANT-based) FLUKA-2002 code is a general purpose Monte Carlo code for studying transport and interactions of particles in a material over a wide energy range. The program is best known for its hadron event generators; the used version of the code can also handle (with similar or better accuracy) muons, low-energy neutrons, and electromagnetic effects. Figure 21 (left panel) indicates good agreement of the results of the simulation with NPOL efficiencies extracted from E93-038 data [Semenova et al. (2003)]. Both simulation and data analysis were made for the front (rear) array threshold of 8 (20) MeVee. Simulating the analyzing power (A_Y) for E93-038 polarimeter, for elastic n - p and quasielastic scattering events in the front array, we determined (*in the rest frame of the target nucleon*) A_Y values from the partial-wave analysis embodied in the Scattering Analysis Interactive Dial-In (SAID) code [Arndt (1977, 2000)]. In our simplified approach, we supposed that $A_Y = 0$ for both inelastic

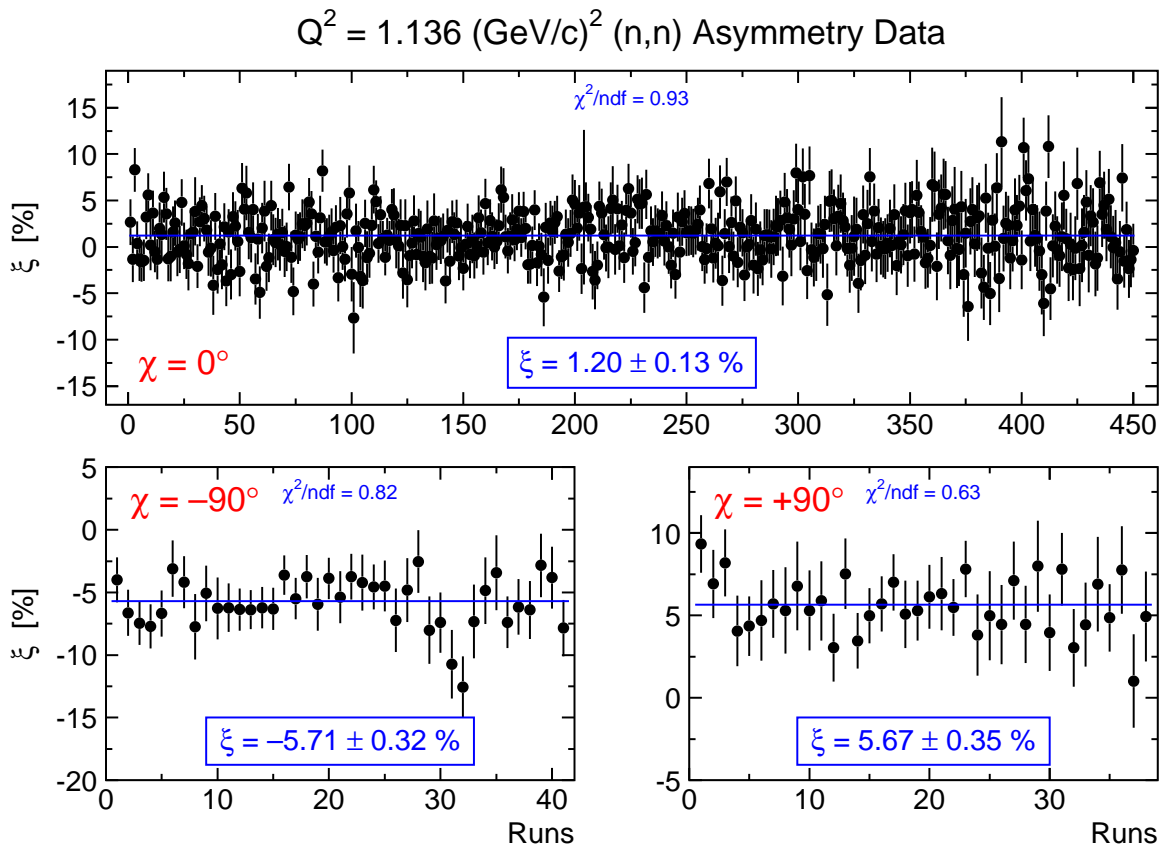


Figure 18: Asymmetries obtained from the analysis of E93-038 data at $Q^2 = 1.13 \text{ (GeV/c)}^2$.

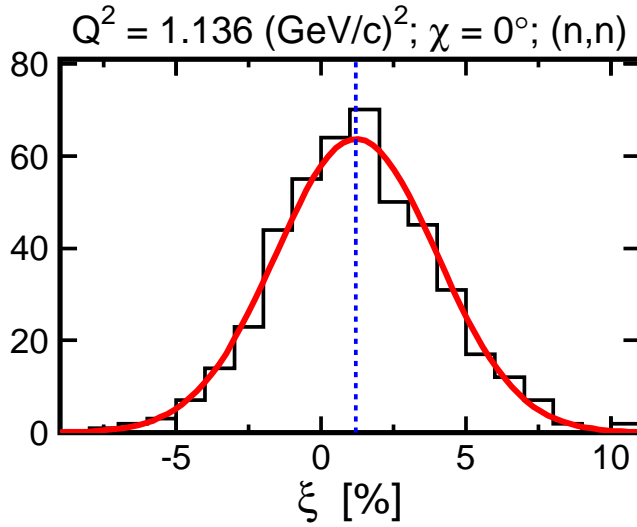


Figure 19: Histogram of E93-038 asymmetries at $Q^2 = 1.13 \text{ (GeV/c)}^2$ ($\chi = 0^\circ$). The red solid curve is a Gaussian fit, and the blue dashed line is the mean value of the asymmetry from the Fig. 18.

reactions and multiple scattering events. Probably, this assumption leads to the disagreement between the simulated (and averaged over the NPOL acceptance) and the measured analyzing power at the low neutron energy of 239 MeV. Nevertheless, at higher neutron energies ($T_n = 608$ and 786 MeV), *the simulated and measured in E93-038 A_Y values are in very good agreement* (see right panel in Fig. 21).

The beam polarization measured in March 2001 is plotted in Fig. 22. The mean polarization during this two-weeks period was 82.2 ± 0.1 (-81.0 ± 0.2)% with the $\lambda/2$ wave plate “OUT” (“IN”).

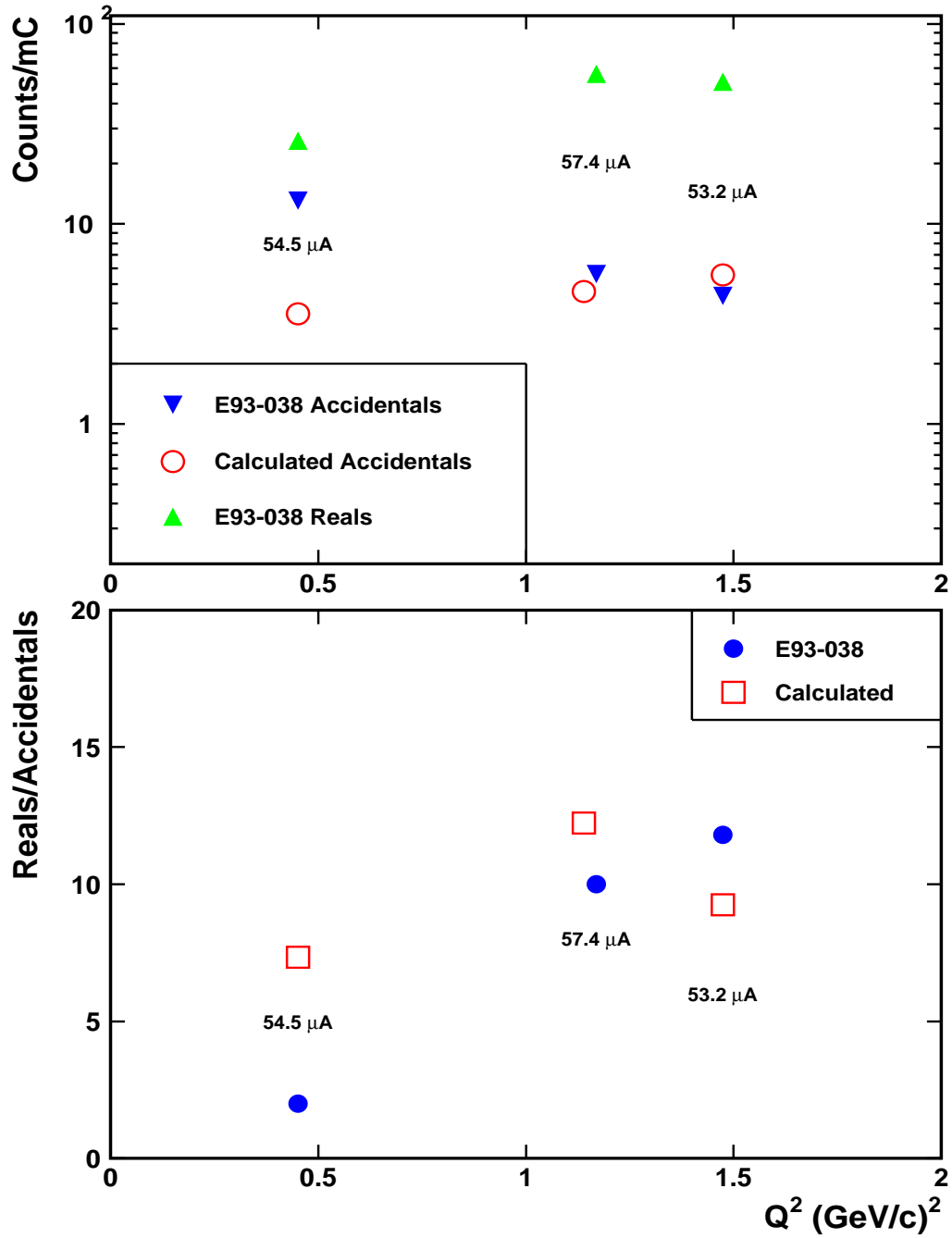


Figure 20: Real event rate, accidental coincidence rate, and the reals-to-accidentals ratio obtained from E93-038. The target-front array flight path was 7 m for NPOL at 46 degrees.

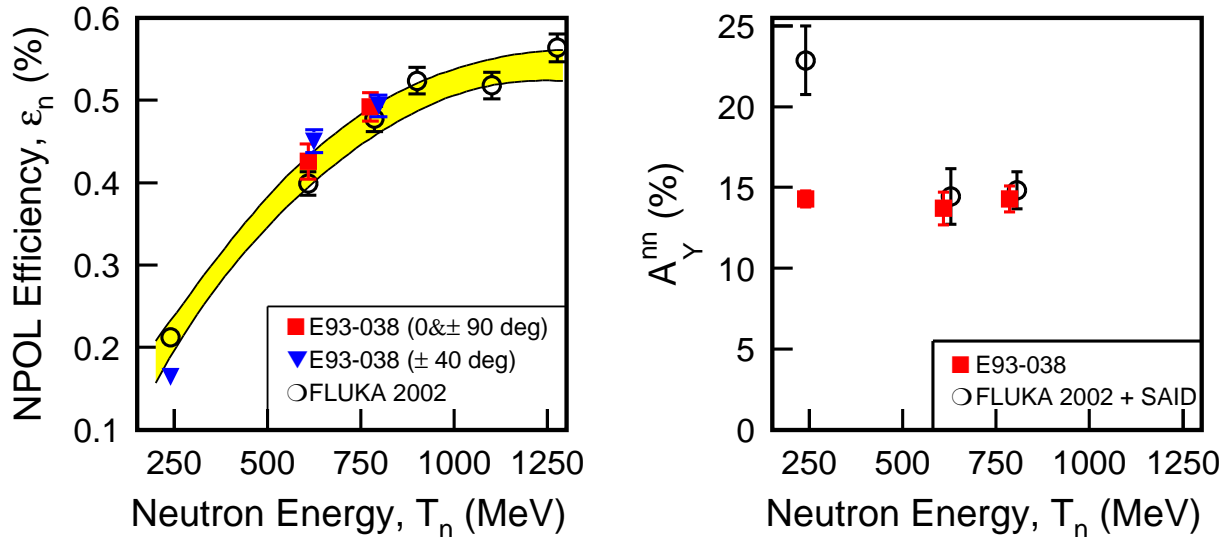


Figure 21: Comparison of the simulated neutron polarimeter parameters (viz., analyzing power, A_Y^n , and the neutron polarimeter efficiency, ϵ_n) with the results from E93-038. Yellow band in the left panel shows an uncertainty on the fit of the simulated efficiencies with a polynomial function.

5 Beam Time

As shown in Table 3, we estimate that a total data acquisition time of 37 days will be needed to produce a statistical uncertainty ΔG_E^n in the vicinity of 0.0032 at each of two Q^2 points [viz., 3.0 and 4.0 (GeV/c)²]. Also needed will be five days of commissioning time with beam to check out the spectrometer, the Moeller polarimeter, and the neutron polarimeter [NPOL] and electronics. NPOL checkout includes checking all detectors and detector thresholds, adjusting timing, adjusting the thickness of the Pb curtain and determining the optimal beam current, and checking room background with a shadow shield. Seven days will be required without beam for pulse-height calibrations and cosmic ray tests of the polarimeter detectors.

The projection was based on a calculation of a fraction of electron-neutron coincidence events corrupted from a background particle (charged or neutral) that appears during a coincidence time window of 20 ns. For a 75 (55) μA beam at $Q^2 = 3.0$ (4.0) (GeV/c)², the corrupted fraction is calculated to be about 20% (see Fig. 13). The estimated acquisition times for runs on a 15-cm LH_2 target will be needed to assess the false asymmetry or dilution from the two-step process $d(\vec{e}, e' \vec{p})_n + \text{Pb}(\vec{p}, \vec{n})$.

Our beam-time request for measuring at $Q^2 = 3.0$ and 4.0 (GeV/c)² is shown in Table 3.

The proposed measurements can be done also in Hall A. It turns out that the counting rates are essentially the same. This collaboration is willing to run in Hall A if the experiment can be scheduled earlier in Hall A than in Hall C.

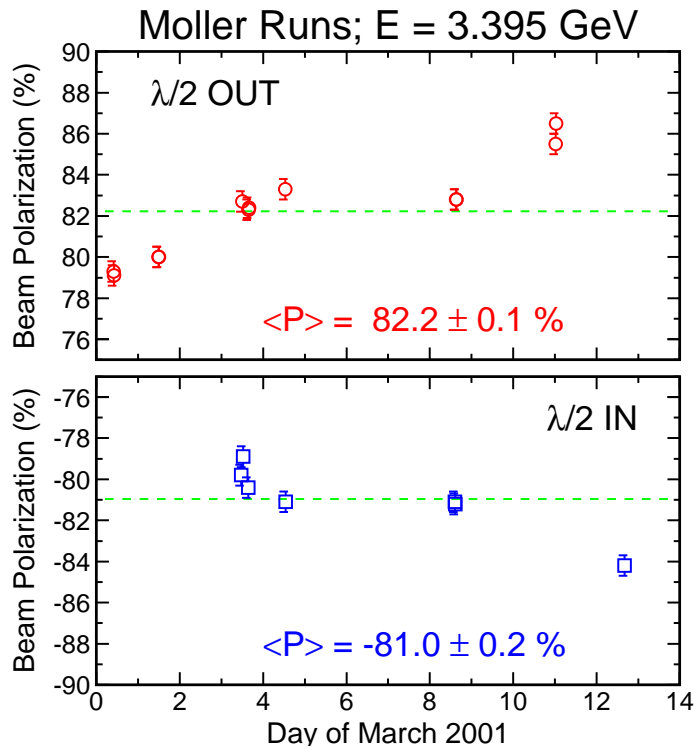


Figure 22: Electron beam polarization in March 2001.

6 Collaboration

Each of the participants listed earlier contributed to the success of E93-038. The collaboration is a strong, experienced, and large team (currently about 70 scientists from 24 institutions). Graduate students will be added after the proposed experiment is approved and scheduled. As in E93-038, Kent State University (KSU) will be responsible for the neutron polarimeter; MIT, for the neutron spin-precession dipole magnet [CHARYBDIS]; and JLab for the magnetic spectrometer [HMS]. KSU provided the neutron detectors in the rear array and the polarimeter electronics; Hampton University provided ten of the neutron detectors in the front array, while JLab provided another ten. We are requesting JLab to provide another ten of these 10-cm×10-cm×100-cm detectors. The University of Virginia provided the tagger detectors used in E93-038. Duke University took responsibility for the Analysis Engine and also for setting up the electronics and timing. Professor James J. Kelly at the University of Maryland spearheaded the development of the analysis programs used in E93-038, and Dr. A.Yu. Semenov functioned as the coordinator of the E93-038 analysis effort. T. Reichelt (Bonn), H. Fenker (JLab), and S. Danagoulian (NCAT) were the lead scientists in establishing the operating conditions for running the Moeller polarimeter at a beam energy below one GeV, and in setting up and running the Moeller polarimeter at the two higher energies. A. Ahmidouch (NCAT) and S. Taylor (MIT) were the lead scientists in mapping the CHARYBDIS dipole magnet. For this proposal, the personnel at the same institutions will provide their expertise. With respect to equipment, we anticipate the need for 24 additional 10-in×40-in×4-in neutron detectors in order to replace the 12 20-in×40-in×4-in detectors in the rear array. Kent State University can provide 12

G_E^n physics measurements Q^2 [(GeV/c) ²]	3.0	4.0	Totals
LD_2 target	7	21	28
LH_2 target	1	1	2
Dummy target	1	1	2
Beam polarization	1	1	2
Time calibrations [LD_2 target]	1	1	2
Overhead ^(a)	0.5	0.5	1
Total physics measurements	11.5	25.5	37

Table 3: Beam-time [days] for measuring at $Q^2 = 3.0$ and 4.0 (GeV/c)² for a 75 (55) μ A, 80% polarized beam on a 15-cm LD_2 target.

(a) 144 changes in Charybdis dipole current, 72 target changes, starting and stopping the DAQ system at least 850 times for runs that are typically 2 hours long.

of these 24, and we are requesting JLab to provide the other 12 to replace each 20-in \times 40-in \times 4-in detector with two 10-in \times 40-in \times 4-in detectors in E93-038. A recent price quote from Saint-Gobain [Bicron] for scintillators is \$1468 for each 10-in \times 4-in \times 40-in bar and \$670 for each 10-cm \times 10-cm \times 100-cm bar. KSU will assemble and test the detectors. New electronics needs for the enhanced polarimeter include 9 quad constant fraction discriminators, 36 (400 ns) delay lines, 24 preamps, an additional control box, and light pipes and 2-in PMT's for the 10-cm \times 10-cm \times 100-cm detectors, and replacement 5-in PMT's for the detectors in the rear array. We are requesting JLab to provide the quad constant-fraction discriminators, the delay lines and the PMT's. KSU would provide the remainder. In the enhanced polarimeter, we plan to use multi-hit TDC's, which we understand will be available.

References

- [Arenhoevel 1987] H. Arenhoevel, Phys. Lett. **B199**, 13 (1987).
- [Arenhoevel 1988] H. Arenhoevel *et al.*, Z. Phys. **A331**, 123 (1988).
- [Arenhoevel 2002] H. Arenhoevel, private communication (2002).
- [Arndt 1977] R.A. Arndt, R.H. Hackman, and L.D. Roper, Phys. Rev. **C15** 1002 (1977).
- [Arndt 2000] R. A. Arndt, L. D. Roper *et al.*, Scattering Analysis Interactive Dial-In (SAID) Program. Virginia Polytechnic Institute and State University, Unpublished. The Virginia Tech Partial-Wave Analysis Facility is still available from the original web site <http://said.phys.vt.edu/>. This facility is available on-line at <http://www.gwdac.phys.gwu.edu/> from the CNS Data Analysis Center at The George Washington University.
- [Aznaurian 1993] I.G. Aznaurian, Phys. Lett. **B316**, 391 (1993).
- [Beck 1992] G. Beck and H. Arenhoevel, Few Body Systems **13**, 165 (1992).
- [Bermuth 2003] J. Bermuth *et al.*, Phys. Lett. **B564**, 199 (2003) updates D. Rohe *et al.*, Phys. Rev. Lett. **83**, 4257 (1999).
- [Bijker 2003] R. Bijker and F. Iachello, private communication (2003).
- [Boffi 2002] S. Boffi, L. Ya. Glozman, W. Klink, W. Plessas, M. Radici, and R. F. Wagenbrunn, Eur. Phys. J. A **14**, 17 (2002); W. Plessas, S. Boffi, L. Ya. Glozman, W. Klink, M. Radici, and R. F. Wagenbrunn, Nucl. Phys. A **699**, 312c (2002); R. F. Wagenbrunn, S. Boffi, W. Klink, W. Plessas, and M. Radici, Phys. Lett. B **511**, 33 (2001).
- [Brun 1993] R. Brun *et al.* *GEANT Detector Description and Simulation Tool*. CERN Program Library Long Writeup W5013, September, 1993.
- [Cardarelli 2000] F. Cardarelli, S. Simula, Phys. Rev. **C62**, 065201 (2000); S. Simula (private communication).
- [Cecil 1979] R. Cecil, B.D. Anderson, R. Madey. Nucl. Instrum. Meth. **161**, 439 (1979).
- [Chung 1991] P.L. Chung and F. Coester, Phys. Rev. **D44**, 229 (1991).
- [Degtyarenko 1992] P.V. Degtyarenko, M.V. Kossov. *Monte Carlo Program for Nuclear Fragmentation*. Preprint ITEF 11-92, Moskow (1992).
- [Degtyarenko 2000] P.V. Degtyarenko, M.V. Kossov, and H.-P. Wellisch. *Chiral invariant phase space event generator*. Eur. Phys. J. A **8**, 217-222 (2000); A **9**, 411-420 (2000); A **9**, 421-424 (2000).
- [Dong 1998] S.J. Dong, K.F. Liu, and A.G. Williams, Phys. Rev. **D58**, 074504 (1998).
- [Drechsel 1989] D. Drechsel and M.M. Giannini, Rep. Prog. Phys. **52**, 1083 (1989).

- [Dytman 1987] S. Dytman, private communication (1987).
- [Eden 1994] T. Eden *et al.*, Phys. Rev. **C50**, R1749 (1994).
- [Fasso 2001] A. Fasso, A. Ferrari, P.R. Sala, Electron-Photon Transport in FLUKA: Status, Proceedings of the Monte Carlo 2000 Conference, Lisbon, October 23-26, 2000, A. Kling, F. Barao, M. Nakagawa, L. Tavora, P. Vaz eds., Springer-Verlag Berlin, pp. 159-164 (2001).
- [Fasso 2001a] A. Fasso, A. Ferrari, J. Ranft, P.R. Sala, FLUKA: Status and Perspective for Hadronic Applications, Proceedings of the Monte Carlo 2000 Conference, Lisbon, October 23-26, 2000, A. Kling, F. Barao, M. Nakagawa, L. Tavora, P. Vaz eds., Springer-Verlag Berlin, pp. 955-960 (2001).
- [Feshbach 1967] H. Feshbach and E. Lomon, Rev. Mod. Phys. **39**, 611 (1967).
- [Frank 1996] M.R. Frank, B.K. Jennings, and G.A. Miller, Phys. Rev. **C54**, 920 (1996).
- [Friar 1990] J.L. Friar, Phys. Rev. **C42**, 2310 (1990).
- [Gari 1985] M.F. Gari and W. Krumpelmann, Z. Phys. **A322**, 689 (1985).
- [Gari 1992] M.F. Gari and W. Krumpelmann, Phys. Lett. **B274**, 159 (1992).
- [Galster 1971] S. Galster, H. Klein, J. Moritz, K.H. Schmidt, D. Wegener, and J. Bleckwenn, Nucl. Phys. **B32**, 221 (1971).
- [Gayou 2002] O. Gayou *et al.*, Phys. Rev. Lett. **88**, 092301 (2002).
- [Golack 2001] J. Golak, G. Ziemer, H. Kamada, H. Witala, and W. Glöckle, Phys. Rev. C **63**, 034006 (2001) applies FSI corrections to J. Becker *et al.*, Eur. Phys. J. A **6**, 329 (1999).
- [Herberg 1999] C. Herberg *et al.*, Eur. Phys. J. **A5**, 131 (1999) applies FSI corrections to M. Ostrick *et al.*, Phys. Rev. Lett. **83**, 276 (1999).
- [Holzwarth 2002] G. Holzwarth, hep-ph/020138; Z. Phys. **A356**, 339 (1996).
- [Iachello 1973] F. Iachello, A.D. Jackson, and A. Lande, Phys. Lett. **43B**, 191 (1973).
- [Iachello 2003] F. Iachello, Proceedings of 4th Int. Conference on Perspectives in Hadronic Physics, Trieste, Italy (2003). To be published in Eur. Phys. J.
- [Isgur 1998] N. Isgur, Phys. Rev. Lett. **83**, 272 (1999).
- [Isgur 2000] N. Isgur and J.W. Negele, Nuclear Theory with Lattice QCD, a proposal to DOE, PI's (2000).
- [Ji 1991] X. Ji, Phys. Lett. **B254**, 456 (1991).
- [Jones 2000] M. Jones *et al.*, Phys. Rev. Lett. **84**, 1398 (2000).
- [Kaskulov (2003)] M.M. Kaskulov and P. Grabmayr, Phys. Rev. C **67**, 042201(R) (2003); nucl-th/0308105; M.M. Kaskulov (private communication).

- [Kelly 2001a] J.J. Kelly, Time Calibration Procedures for E93-038 Polarimeter: Version 2.2, JLab E93-038 internal report (2001),
URL: http://www.physics.umd.edu/enp/e93038/time_calibration.ps
- [Kelly 2003] J.J. Kelly, private communication (2003).
- [Klein 1997a] F. Klein and H. Schmieden, Nucl. Phys. **A623**, 323c (1997).
- [Klein 1997b] F. Klein, Proc. of the 14th Int. Conf. on Particles and Nuclei, ed. by C.E. Carlson and J.J. Domingo, World Scientific 1997, p.121.
- [Kopecky 1997] S. Kopecky *et al.*, Phys. Rev. C **56**, 2229 (1997); Phys. Rev. Lett. **74**, 2427 (1995).
- [Kroll 1992] P. Kroll, M. Schurmann, and W. Schweiger, Z. Phys. **A342**, 429 (1992).
- [Laget 1990] J.M. Laget, Phys. Lett. **B273**, 367 (1990).
- [Liu 2001] K.F. Liu, Private Communication (2001).
- [Lomon 2002] E. L. Lomon, Phys. Rev. C **66**, 045501 (2002); Phys. Rev. C **64**, 035204 (2001).
- [Lu 1998] D.H. Lu, A.W. Thomas, and A.G. Williams, Phys. Rev. **C57**, 2628 (1998).
- [Lung 1993] A. Lung *et al.*, Phys. Rev. Lett. **70**, 718 (1993).
- [Ma 2002] B.-Q. Ma, D. Qing, and I. Schmidt, Phys. Rev. C **65**, 035205 (2002).
- [Madey 1995] R. Madey, A. Lai, and T. Eden, Polarization Phenomena in Nuclear Physics, edited by E.J. Stephenson S.E. Vigeler, AIP Proceedings No. 339, 47-54 (1995).
- [Madey 2003] R. Madey *et al.*, Phys. Rev. Lett. **91**, 122002 (2003).
- [Mergell 1996] P. Mergell, U.G. Meissner, D. Drechsel, Nucl. Phys. **A596**, 367 (1996).
- [Meyerhoff 1994] M. Meyerhoff *et al.*, Phys. Lett. **B327**, 201 (1994).
- [Milbrath 1998] B. D. Milbrath *et al.*, Phys. Rev. Lett. **80**, 452 (1998); Phys. Rev. Lett. **82**, 2221(E) (1999).
- [Miller 2002] G. A. Miller, Phys. Rev. C **66**, 032201(R) (2002); G. A. Miller and M. R. Frank, Phys. Rev. C **65**, 065205 (2002); M. R. Frank, B. K. Jennings, and G. A. Miller, Phys. Rev. C **54**, 920 (1996); G. A. Miller, private communication (2003).
- [Mosconi 1991] B. Mosconi, J. Pauchenwein, and P. Ricci, Proceedings of the XIII European Conference on Few-Body Problems in Physics, Marciana Marina (Elba), Italy (September 1991).
- [Ohlsen 1973] G.G. Ohlsen and P.W. Keaton, Jr., Nucl. Instr. Meth. **109**, 41 (1973).
- [Pace 2000] E. Pace, G. Salme, F. Cardarelli, and S. Simula, Nucl. Phys. **A666**, 33 (2000).

- [Passchier 1999] I. Passchier *et al.*, Phys. Rev. Lett. **82**, 4988 (1999).
- [Platchkov 1990] S. Platchkov *et al.*, Nucl. Phys. **A508**, 343c (1990).
- [Pospischil 2001] Th. Pospischil *et al.*, Eur. Phys. J. A **12**, 125 (2001).
- [Radyushkin 1984] A.V. Radyushkin, Acta Phys. Polon. **B15**, 403 (1984).
- [Rekalo 1989] M.P. Rekalo, G.I. Gakh, and A.P. Rekalo, J. Phys. **G15**, 1223 (1989).
- [De Sanctis 2000] M. De Sanctis, M.M. Giannini, L. Repetto, and E. Santopinto, Phys. Rev. **C62**, 025208 (2000).
- [Schiavilla 2001] R. Schiavilla and I. Sick, Phys. Rev. **C64**, 041002 (2001).
- [Schmieden 1996] H. Schmieden, Proc. of the 12th Int. Symposium on High-Energy Spin Physics, Amsterdam (1996), ed. by C.W. de Jager et al., World Scientific 1997, p.538.
- [Semenova 2002] I.A. Semenova, R. Madey, and A.Yu. Semenov, Gain in Figure-of-Merit of the E93-038 Neutron Polarimeter with Passive Converters, JLab E93-038 internal report (2002),
URL: <http://www.jlab.org/~semenov/reports/irina-effConv.ps>
- [Semenova 2003] I.A. Semenova, A.Yu. Semenov, and R. Madey, Simulation of the Efficiency of the E93-038 Neutron Polarimeter with the FLUKA code, JLab E93-038 internal report (2003).
- [Ulmer 1991] P.E. Ulmer, MCEEP – Monte Carlo for Electro-Nuclear Coincidence Experiments, CEBAF–TN–91–101 (1991).
- [Zeitnitz 1994] C. Zeitnitz and T.A. Gabriel, Nucl. Instrum. Meth. **A349**, 106 (1994).
- [Zhu 2001] H. Zhu *et al.*, Phys. Rev. Lett. **87**, 081801 (2001).

Measurements of G_E^n/G_M^n from the ${}^2\text{H}(\vec{e}, e'\vec{n}){}^1\text{H}$ Reaction to $Q^2 = 1.45$ (GeV/c) 2

R. Madey,^{1,2} A. Yu. Semenov,¹ S. Taylor,³ B. Plaster,³ A. Aghalaryan,⁴ E. Crouse,⁵ G. MacLachlan,⁶ S. Tajima,⁷ W. Tireman,¹ Chenyu Yan,¹ A. Ahmidouch,⁸ B. D. Anderson,¹ H. Arenhövel,⁹ R. Asaturyan,⁴ O. K. Baker,¹⁰ A. R. Baldwin,¹ D. Barkhuff,^{3,*} H. Breuer,¹¹ R. Carlini,² E. Christy,¹⁰ S. Churchwell,^{7,†} L. Cole,¹⁰ S. Danagoulian,^{2,8} D. Day,¹² T. Eden,^{1,10,‡} M. Elaasar,¹³ R. Ent,² M. Farkhondeh,³ H. Fenker,² J. M. Finn,⁵ L. Gan,¹⁰ K. Garrow,² A. Gasparian,^{8,10} P. Gueye,¹⁰ C. R. Howell,⁷ B. Hu,¹⁰ M. K. Jones,² J. J. Kelly,¹¹ C. Keppel,¹⁰ M. Khandaker,¹⁴ W.-Y. Kim,¹⁵ S. Kowalski,³ A. Lai,¹ A. Lung,² D. Mack,² D. M. Manley,¹ P. Markowitz,¹⁶ J. Mitchell,² H. Mkrtchyan,⁴ A. K. Opper,⁶ C. Perdrisat,⁵ V. Punjabi,¹⁴ B. Raue,¹⁶ T. Reichelt,¹⁷ J. Reinhold,¹⁶ J. Roche,⁵ Y. Sato,¹⁰ N. Savvinov,¹¹ I. A. Semenova,¹ W. Seo,¹⁵ N. Simicevic,¹⁸ G. Smith,² S. Stepanyan,^{4,15} V. Tadevosyan,⁴ L. Tang,¹⁰ P. E. Ulmer,¹⁹ W. Vulcan,² J. W. Watson,¹ S. Wells,¹⁸ F. Wesselmann,¹² S. Wood,² Chen Yan,² S. Yang,¹⁵ L. Yuan,¹⁰ W.-M. Zhang,¹ H. Zhu,¹² and X. Zhu¹⁰

(The Jefferson Laboratory E93-038 Collaboration)

¹Kent State University, Kent, Ohio 44242, USA

²Thomas Jefferson National Accelerator Facility, Newport News, Virginia 23606, USA

³Massachusetts Institute of Technology, Cambridge, Massachusetts 02139, USA

⁴Yerevan Physics Institute, Yerevan 375036, Armenia

⁵The College of William and Mary, Williamsburg, Virginia 23187, USA

⁶Ohio University, Athens, Ohio 45701, USA

⁷Duke University and TUNL, Durham, North Carolina 27708, USA

⁸North Carolina A&T State University, Greensboro, North Carolina 27411, USA

⁹Johannes Gutenberg-Universität, D-55099 Mainz, Germany

¹⁰Hampton University, Hampton, Virginia 23668, USA

¹¹University of Maryland, College Park, Maryland 20742, USA

¹²University of Virginia, Charlottesville, Virginia 22904, USA

¹³Southern University at New Orleans, New Orleans, Louisiana 70126, USA

¹⁴Norfolk State University, Norfolk, Virginia 23504, USA

¹⁵Kyungpook National University, Taegu 702-701, Korea

¹⁶Florida International University, Miami, Florida 33199, USA

¹⁷Rheinische Friedrich-Wilhelms-Universität, D-53115 Bonn, Germany

¹⁸Louisiana Tech University, Ruston, Louisiana 71272, USA

¹⁹Old Dominion University, Norfolk, Virginia 23529, USA

(Received 27 June 2003; published 19 September 2003)

We report new measurements of the ratio of the electric form factor to the magnetic form factor of the neutron, G_E^n/G_M^n , obtained via recoil polarimetry from the quasielastic ${}^2\text{H}(\vec{e}, e'\vec{n}){}^1\text{H}$ reaction at Q^2 values of 0.45, 1.13, and 1.45 (GeV/c) 2 with relative statistical uncertainties of 7.6% and 8.4% at the two higher Q^2 points, which points have never been achieved in polarization measurements.

DOI: 10.1103/PhysRevLett.91.122002

PACS numbers: 14.20.Dh, 13.40.Gp, 24.70.+s, 25.30.Bf

The nucleon elastic electromagnetic form factors are fundamental quantities needed for an understanding of nucleon and nuclear structure. The evolution of the electric and magnetic form factors with Q^2 , the square of the four-momentum transfer, is related to the charge and current distributions within the nucleon. Precision measurements of the electromagnetic form factors are important for tests of nonperturbative quantum chromodynamics (QCD) either on the lattice or in models. With the advent of high duty-factor polarized electron beam facilities, experiments employing recoil polarimeters [1,2], polarized ${}^3\text{He}$ targets [3–5], and polarized deuterium targets [6,7] have yielded the first precision measurements of G_E^n , the neutron electric form factor. These

polarization measurements of G_E^n are limited to $Q^2 \leq 0.67$ (GeV/c) 2 and are, within errors, consistent with the Galster parametrization [8].

In the plane-wave approximation, the recoil polarization produced by a longitudinally polarized electron beam in quasielastic electron-neutron scattering is restricted to the scattering plane [9,10]: The longitudinal component, $P_{L'}$, and the transverse (sideways) component, $P_{S'}$, are parallel and perpendicular, respectively, to the recoil neutron's momentum vector. In terms of G_E^n and G_M^n , $P_{S'}$ and $P_{L'}$ can be written as

$$P_{S'}/P_{L'} = -K_S G_E^n G_M^n / I_0, \quad (1)$$

$$P_{L'}/P_L = K_L(G_M^n)^2/I_0, \quad (2)$$

where P_L is the electron beam polarization, $I_0 \equiv (G_E^n)^2 + K_0(G_M^n)^2$, and K_S , K_L , and K_0 are kinematic functions of the electron scattering angle, θ_e , and Q^2 . Measurements of P_S and $P_{L'}$ via a secondary analyzing reaction permit an extraction of the ratio of G_E^n to G_M^n ; a significant advantage of this technique is that P_L and the analyzing power of the secondary reaction cancel in the polarization ratio $P_S/P_{L'}$. Also, for quasifree emission, Arenhövel [11] demonstrated that P_S and $P_{L'}$ are insensitive to final state interactions (FSI), meson exchange currents (MEC), isobar configurations (IC), and to theoretical models of deuteron structure.

In this Letter, we report new measurements of G_E^n/G_M^n obtained via recoil polarimetry from the quasielastic ${}^2\text{H}(\vec{e}, e'\vec{n})\text{H}$ reaction at three central Q^2 values of 0.45, 1.15, and 1.47 $(\text{GeV}/c)^2$. Our measurements were carried out in Hall C of the Thomas Jefferson National Accelerator Facility. The experimental arrangement with an isometric view of our polarimeter is shown in Fig. 1. A beam of longitudinally polarized electrons (with a typical polarization of 80%) scattered quasielastically from a neutron in a 15-cm liquid deuterium target. A scattered electron was detected in the High Momentum Spectrometer (HMS) in coincidence with the recoil neutron. The neutron polarimeter (NPOL) was used to measure the up-down scattering asymmetry from the transverse component of the recoil neutron polarization presented to the polarimeter. To permit measurements of the up-down scattering asymmetry from different combinations of P_S and $P_{L'}$, a dipole magnet (Charybdis) located in front of the polarimeter precessed the recoil neutron's polarization vector through an angle χ .

The polarimeter consisted of a total of 44 plastic scintillation detectors. To achieve luminosities of $\sim 3 \times 10^{38} \text{ cm}^{-2} \text{ s}^{-1}$, the front array was segmented into 20 detectors $[100 \text{ cm} \times 10 \text{ cm} \times 10 \text{ cm}]$. Top and bottom rear arrays were shielded from the direct path of particles from the target. Each rear array consisted of six “20-in”

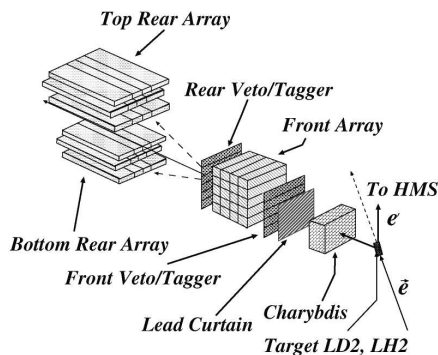


FIG. 1. A schematic diagram of the polarimeter.

detectors $[101.6 \text{ cm} \times 50.8 \text{ cm} \times 10.16 \text{ cm}]$ and six “10-in” detectors $[101.6 \text{ cm} \times 25.4 \text{ cm} \times 10.16 \text{ cm}]$. A double layer of “veto/tagger” detectors (each 0.64-cm thick) directly ahead of and behind the front array identified incoming and scattered charged particles. A 10-cm lead curtain attenuated the flux of electromagnetic radiation and charged particles incident on the polarimeter. The flight path from the center of the target to the center of the front array was 7.0 m, and the mean flight path from the front array to the rear array was 2.5 m.

For a fixed neutron scattering angle of 46.0° , central Q^2 values of 0.45 and 1.47 $(\text{GeV}/c)^2$ were associated with beam energies of 0.884 and 3.40 GeV, respectively, and electron scattering angles of 52.7° and 23.6° , respectively. The measurement conducted at a central Q^2 value of 1.15 $(\text{GeV}/c)^2$ was associated with two beam energies of 2.33 and 2.42 GeV and electron scattering angles of 30.8° and 30.1° , respectively. We conducted asymmetry measurements with the polarization vector precessed through $\chi = \pm 40^\circ$ at each of our Q^2 points; in addition, at $Q^2 = 1.15$ and 1.47 $(\text{GeV}/c)^2$, we conducted asymmetry measurements with the polarization vector precessed through $\chi = 0^\circ, \pm 90^\circ$. The acceptance-averaged values of Q^2 are $\langle Q^2 \rangle = 0.45, 1.13, \text{ and } 1.45 \text{ (GeV}/c)^2$.

Typical time-of-flight spectra are shown in Fig. 2. The left panel is an HMS-NPOL coincidence time-of-flight spectrum. We compared the measured time of flight, cTOF, with the time of flight calculated from electron kinematics and offsets determined by a calibration procedure; the result is centered on zero with a FWHM of approximately 1.5 ns. The right panel is the time-of-flight spectrum between a neutron event in the front array and an event in the top or bottom rear array. We compared this measured time of flight, ΔTOF , with the time of flight calculated for elastic np scattering. Variations with respect to a nominal 2.5 m flight path were compensated. The tail on the slow side is due to Fermi motion in carbon and nuclear reactions, and the secondary peak at ~ -2.5 ns is the result of π^0 production in the front array. To extract the physical scattering asymmetry, we calculated the cross ratio, r , which is defined to be the ratio of two geometric means, $(N_U^+ N_D^-)^{1/2}$ and

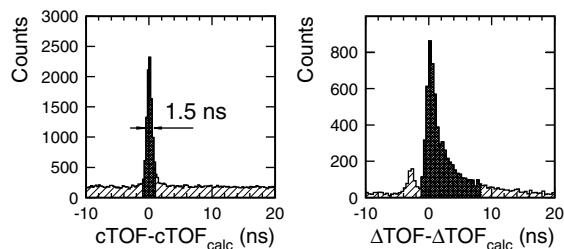


FIG. 2. Typical time-of-flight spectra for $Q^2 = 1.15 \text{ (GeV}/c)^2$. Selected portions are shaded.

$(N_U^- N_D^+)^{1/2}$, where $N_U^+ (N_D^-)$ is the yield in the Δ TOF peak for neutrons scattered up (down) when the beam helicity was positive (negative); the yields, corrected for background, were obtained by peak fitting. The physical scattering asymmetry is then given by $(r - 1)/(r + 1)$. The merit of the cross ratio technique [12] is that the neutron polarimeter results are independent of the luminosities for positive and negative helicities, and the efficiencies and acceptances of the top and bottom halves of the polarimeter. Beam charge asymmetries (of typically 0.1%) and detector threshold differences cancel in the cross ratio.

To account for the finite experimental acceptance and nuclear physics effects such as FSI, MEC, and IC, we averaged Arenhövel's theoretical ${}^2\text{H}(\vec{e}, e'\vec{n})^1\text{H}$ calculations [13] over the experimental acceptance. These calculations include leading-order relativistic contributions to a nonrelativistic model of the deuteron as an n - p system, employ the Bonn R -space NN potential [14] for the inclusion of FSI, and include MEC and IC. Other realistic potentials (e.g., the Argonne V18 [15]) give essentially the same results. Recoil polarizations were calculated over a kinematic grid; we used multidimensional interpolation to compute the polarizations between the grid elements.

To average these theoretical calculations over the experimental acceptance, we prepared two independent simulation programs. First, we developed the GENGEN Monte Carlo simulation program, which includes an event generator and detailed models of the electron spectrometer and the neutron polarimeter. GENGEN reproduces experimental kinematic distributions and models the response of the polarimeter. Second, we developed a program that used the kinematics of the reconstructed quasielastic events from the experimental data to compute the recoil polarization for each event used in the data analysis; the advantage of this method is that it does not require a model of the experimental acceptance.

For the first-pass analysis, the simulation programs used theoretical calculations that assumed the Galster parametrization for G_E^n with different multiplicative factors. We determined the optimal factor for each Q^2 that provided the best agreement between the simulated polarization ratios and the experimental asymmetry ratios. Next, we fitted the current world data [1,2,4–7,16,17] and our first-pass acceptance and nuclear physics corrected results for G_E^n to a Galster parametrization with two free parameters. Then we repeated the simulations using new

TABLE I. Estimated systematic uncertainties in $\Delta g/g$ [%].

Source	$\langle Q^2 \rangle$ [(GeV/c) ²]				
	0.45 ^a	1.13 ^a	1.13 ^b	1.45 ^a	1.45 ^b
Beam polarization	1.4	0.8	0.4	1.7	0.3
Charge exchange	<0.01	0.02	0.06	<0.01	0.2
Depolarization	<0.1	<0.1	0.2	0.1	0.6
Positioning/traceback	0.2	0.3	0.3	0.4	0.4
Precession angle	1.1	0.3	0.1	0.5	0.1
Radiative corrections	0.7	0.1	0.1	0.05	0.05
Total of above sources	1.9	0.9	0.5	1.8	0.8

^a $\chi = \pm 40^\circ$ precession.^b $\chi = 0^\circ, \pm 90^\circ$ precession.

theoretical calculations that assumed this modified Galster parametrization for G_E^n . As in the first-pass analysis, we determined the optimal factor that provided the best agreement between simulation and experiment. The differences between these analyses were negligible, and the results from the two simulation programs agreed to better than 2%.

The estimated values of the systematic uncertainties are listed in Table I. A significant advantage of our experimental technique is that the scale and systematic uncertainties are small; the analyzing power of the polarimeter cancels in the polarization ratio, and the beam polarization, P_L , also cancels as it varied little during sequential measurements of the scattering asymmetries. We measured the beam polarization with a Möller polarimeter [18], and changes in P_L were typically $\sim 1\%$ – 2% . The helicity of the beam was reversed at a frequency of 30 Hz to eliminate instrumental asymmetries.

A false asymmetry or a dilution of the asymmetry may arise from the two-step process ${}^2\text{H}(\vec{e}, e'\vec{n})^1\text{H} + \text{Pb}(\vec{p}, \vec{n})$; the contamination from this process was assessed by running with a liquid hydrogen target. The contamination levels are negligible ($\leq 0.3\%$) for $\chi = \pm 40^\circ$ and $\pm 90^\circ$ at all of our Q^2 points, and for $\chi = 0^\circ$, the contamination levels are $\sim 0.3\%$ and $\sim 3\%$ at $\langle Q^2 \rangle = 1.13$ and 1.45 (GeV/c)², respectively; accordingly, we have not corrected our $\langle Q^2 \rangle = 0.45$ and 1.13 (GeV/c)² data for contamination from this two-step process. The net correction obtained for the analysis of all of the data for $\langle Q^2 \rangle = 1.45$ (GeV/c)² [viz., for $\chi = 0^\circ, \pm 40^\circ$, and $\pm 90^\circ$] amounted to $1.3\% \pm 0.1\%$. In addition to charge-exchange reactions in the lead curtain, the flux of neutrons entering the polarimeter may be depolarized as a result of nuclear interactions in the lead curtain.

TABLE II. Results for $g = G_E^n/G_M^n$ and G_E^n . [The first set of errors is statistical, and the second set is systematic.]

$\langle Q^2 \rangle$ [(GeV/c) ²]	$g = G_E^n/G_M^n$	$G_M^n/\mu_n G_D$ [20]	G_E^n
0.447	$-0.0761 \pm 0.0083 \pm 0.0021$	1.003 ± 0.006	$0.0550 \pm 0.0060 \pm 0.0016$
1.132	$-0.131 \pm 0.010 \pm 0.003$	1.057 ± 0.017	$0.0394 \pm 0.0029 \pm 0.0012$
1.450	$-0.190 \pm 0.016 \pm 0.004$	1.044 ± 0.024	$0.0411 \pm 0.0035 \pm 0.0013$

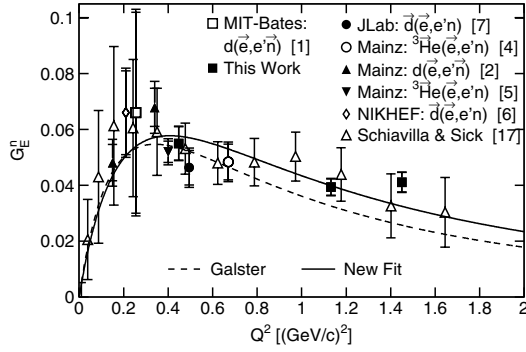


FIG. 3. The current world data on G_E^n versus Q^2 extracted from polarization measurements and an analysis of the deuteron quadrupole form factor [1,2,4-7,17].

Depolarization processes were simulated in GENGEN using a spin-dependent multiple-scattering algorithm employing quasifree scattering from a Fermi gas. The effects of depolarization cancel in the polarization ratio, and the residual noncancellation effect upon g of less than 0.6% is included in the systematic uncertainty.

Afanasev *et al.* [19] calculated radiative corrections to the polarization-transfer coefficients, P_S/P_L and P_L/P_L . The primary effect is depolarization of the electron such that both polarization-transfer coefficients should be increased by $\sim 1.9\%$, $\sim 3.7\%$, and $\sim 4.4\%$ at $\langle Q^2 \rangle = 0.45$, 1.13, and 1.45 $(\text{GeV}/c)^2$, respectively; however, these effects nearly cancel in the polarization ratio such that the net effect upon g is small at $\langle Q^2 \rangle = 0.45$ $(\text{GeV}/c)^2$ and negligible at the two higher Q^2 points.

The values of g and G_E^n that we report are listed in Table II. To determine our values for G_E^n , we used the best-fit values for G_M^n (listed in Table II) obtained using the methods described in [20]. The quoted systematic uncertainties include a 2% uncertainty that results when different data are used for the time calibration.

Our values for G_E^n are plotted in Fig. 3 together with the current world data on G_E^n [1,2,4-7,17] extracted from polarization measurements and an analysis of the deuteron quadrupole form factor [17]. We fitted these data and the G_E^n slope at the origin as measured via low-energy neutron scattering from electrons in heavy atoms [16] to a Galster parametrization: $G_E^n = -a\mu_n\tau G_D/(1+b\tau)$, where $\tau = Q^2/4M_n^2$, $G_D = (1+Q^2/\Lambda^2)^{-2}$, and $\Lambda^2 = 0.71$ $(\text{GeV}/c)^2$. Our best-fit parameters are $a = 0.888 \pm 0.023$ and $b = 3.21 \pm 0.33$.

Polarization measurements of G_E^p/G_M^p [21-24] and G_E^n/G_M^n [1,2,4-7,17] are compared with predictions of selected models in Fig. 4. The chiral soliton model [25] reproduces the dramatic linear decrease observed in $\mu_p G_E^p/G_M^p$ for $1 < Q^2 < 6$ $(\text{GeV}/c)^2$; however, this model fails to reproduce the neutron data at large Q^2 . The light-cone diquark model [26] achieves qualitative

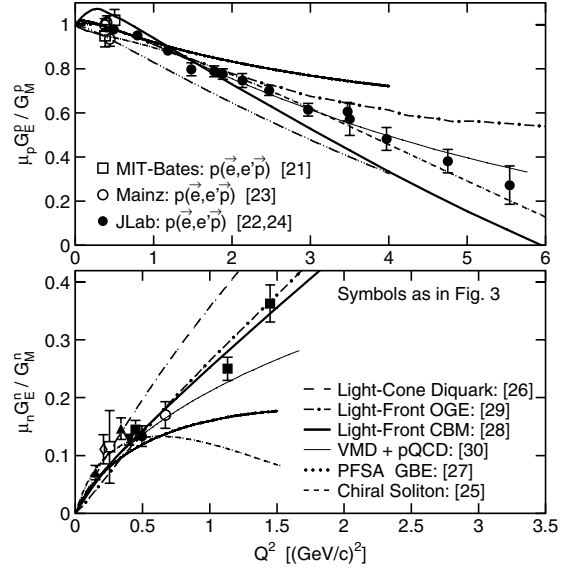


FIG. 4. Predictions of selected models (see text) for $\mu_p G_E^p/G_M^p$ and $\mu_n G_E^n/G_M^n$ compared with proton [21-24] and neutron [1,2,4-7] data.

agreement with the low Q^2 proton and neutron data; however, at high Q^2 , it lies below (above) the proton (neutron) data. A calculation using the pointform spectator approximation (PFSA) with pointlike constituent quarks and a Goldstone boson exchange interaction fitted to the meson and baryon spectrum [27] also achieves qualitative agreement with the low Q^2 proton and neutron data; however, it also fails to describe the high Q^2 proton and neutron data. A light-front calculation using pointlike constituent quarks surrounded by a cloud of pions [28] describes the neutron data, but falls below the proton data at high Q^2 . A one-gluon exchange light-front calculation using constituent quark form factors fitted to $Q^2 < 1$ $(\text{GeV}/c)^2$ data [29] agrees with the neutron data, but deviates from the proton data above $Q^2 \sim 3.5$ $(\text{GeV}/c)^2$. Finally, fits that couple vector meson dominance with the predictions of perturbative QCD [30] agree with the entire range of the proton data, but fall below the neutron data above $Q^2 \sim 1.2$ $(\text{GeV}/c)^2$.

A successful model of confinement must be able to predict both neutron and proton electromagnetic form factors simultaneously. The neutron electric form factor is especially sensitive to small components of the nucleon wave function, and differences between model predictions for G_E^n tend to increase rapidly with Q^2 . Our new G_E^n data provide a challenging test for confinement models and invite extensions to higher Q^2 .

We thank the TJNAF Hall C scientific and engineering staff for their outstanding support. Also, we thank A. Afanasev for providing calculations of the radiative

correction uncertainties. This work was supported in part by the National Science Foundation, the U.S. Department of Energy, and the Deutsche Forschungsgemeinschaft. The Southeastern Universities Research Association (SURA) operates the Thomas Jefferson National Accelerator Facility under the U.S. Department of Energy Contract No. DE-AC05-84ER40150.

*Present Address: Renaissance Technologies, 600 Route 25A, East Setauket, New York 11733, USA.

†Present Address: Department of Physics and Astronomy, University of Canterbury, Private Bag 4800, Christchurch 8020, New Zealand.

‡Present Address: Atmospheric Chemistry Division, National Center for Atmospheric Research, Boulder, Colorado 80307, USA.

- [1] T. Eden *et al.*, Phys. Rev. C **50**, R1749 (1994).
- [2] C. Herberg *et al.*, Eur. Phys. J. A **5**, 131 (1999) applies FSI corrections to M. Ostrick *et al.*, Phys. Rev. Lett. **83**, 276 (1999).
- [3] M. Meyerhoff *et al.*, Phys. Lett. B **327**, 201 (1994).
- [4] J. Bermuth *et al.*, Phys. Lett. B **564**, 199 (2003) updates D. Rohe *et al.*, Phys. Rev. Lett. **83**, 4257 (1999).
- [5] J. Golak, G. Ziemer, H. Kamada, H. Witala, and W. Glöckle, Phys. Rev. C **63**, 034006 (2001) applies FSI corrections to J. Becker *et al.*, Eur. Phys. J. A **6**, 329 (1999).
- [6] I. Passchier *et al.*, Phys. Rev. Lett. **82**, 4988 (1999).
- [7] H. Zhu *et al.*, Phys. Rev. Lett. **87**, 081801 (2001).
- [8] S. Galster, H. Klein, K. H. Schmidt, D. Wegener, and J. Bleckwenn, Nucl. Phys. B **32**, 221 (1971).
- [9] A. I. Akhiezer and M. P. Rekalo, Sov. J. Part. Nuclei **4**, 277 (1974).
- [10] R. G. Arnold, C. E. Carlson, and F. Gross, Phys. Rev. C **23**, 363 (1981).
- [11] H. Arenhövel, Phys. Lett. B **199**, 13 (1987); H. Arenhövel (private communication).
- [12] G. G. Ohlsen and P. W. Keaton, Jr., Nucl. Instrum. Methods **109**, 41 (1973).
- [13] H. Arenhövel, W. Leidemann, and E. L. Tomusiak, Phys. Rev. C **52**, 1232 (1995); **46**, 455 (1992); Z. Phys. A **331**, 123 (1988); **334**, 363(E) (1989); H. Arenhövel (private communication).
- [14] R. Machleidt, K. Holinde, and Ch. Elster, Phys. Rep. **149**, 1 (1987).
- [15] R. B. Wiringa, V. G. J. Stoks, and R. Schiavilla, Phys. Rev. C **51**, 38 (1995).
- [16] S. Kopecky *et al.*, Phys. Rev. C **56**, 2229 (1997); Phys. Rev. Lett. **74**, 2427 (1995).
- [17] R. Schiavilla and I. Sick, Phys. Rev. C **64**, 041002 (2001).
- [18] M. Hauger *et al.*, Nucl. Instrum. Methods Phys. Res., Sect. A **462**, 382 (2001).
- [19] A. Afanasev, I. Akushevich, and N. Merenkov, Phys. Rev. D **64**, 113009 (2001).
- [20] J. J. Kelly, Phys. Rev. C **66**, 065203 (2002).
- [21] B. D. Milbrath *et al.*, Phys. Rev. Lett. **80**, 452 (1998); **82**, 2221(E) (1999).
- [22] M. K. Jones *et al.*, Phys. Rev. Lett. **84**, 1398 (2000); V. Punjabi *et al.* (to be published).
- [23] Th. Pospischil *et al.*, Eur. Phys. J. A **12**, 125 (2001).
- [24] O. Gayou *et al.*, Phys. Rev. Lett. **88**, 092301 (2002).
- [25] G. Holzwarth, hep-ph/020138; Z. Phys. A **356**, 339 (1996). [Version B2 is shown in Fig. 4.]
- [26] B.-Q. Ma, D. Qing, and I. Schmidt, Phys. Rev. C **65**, 035205 (2002).
- [27] S. Boffi, L. Ya. Glozman, W. Klink, W. Plessas, M. Radici, and R. F. Wagenbrunn, Eur. Phys. J. A **14**, 17 (2002); M. Radici (private communication).
- [28] G. A. Miller, Phys. Rev. C **66**, 032201(R) (2002); G. A. Miller (private communication).
- [29] F. Cardarelli and S. Simula, Phys. Rev. C **62**, 065201 (2000); S. Simula (private communication).
- [30] E. L. Lomon, Phys. Rev. C **66**, 045501 (2002); **64**, 035204 (2001).